# An efficient 2-way shear grillage model solution for bridge RC four-pile caps under wall loading

**Authors:**

Dr Jing Cao
Senior Structural Engineer at HERA, New Zealand
Email: caojin259@gmail.com

Dr Alan G Bloodworth
Associate Professor, School of Engineering, University of Warwick, UK
Email: a.bloodworth@warwick.ac.uk

Dr Ming Xu
Associate Professor, Department of Civil Engineering, Tsinghua University, China
Address:
Email: mingxu@mail.tsinghua.edu.cn

**Abstract**

Reinforced concrete four-pile caps under wall loading occur in heavily-loaded foundations in bridge construction. The failure mode of shear across the full width of the cap may occur in these deep structural elements. A statically determinate two-way grillage model, comprising orthogonal deep beam grillage elements obeying a predetermined test observed deflection pattern and boundary conditions, is established to solve the structure's shear capacity. The model gives more accurate and faster solutions than the traditional strut-and-tie method and commercial non-linear numerical modelling. A key step to solve the model is a linear constitutive (load-deflection) relationship developed for the grillage elements. The grillage model is verified against nine pile cap laboratory experiments at University of Southampton (UoS) and results of a numerical modelling parametric study. A Visual Basic Userform based design software is

developed incorporating the model, enabling engineers to obtain the shear capacity, full field reinforcement stress distribution and cap deflections within seconds.

**Keywords**: bridge foundation, reinforced concrete, pile cap, shear, deep beam deflection, strut-and-tie, wall loading, grillage model, VBA Userform design software, constitutive relationship

**Background**

Reinforced concrete (RC) four-pile caps under wall loading serve as independent bridge foundations or form a basic unit for multi-pile caps for heavily-loaded railway steel bridges, as shown in Fig. 1, identifying its longitudinal and transverse directions (LD, TD). International standards (BSI 2004, 2005; Standards Australia 2009) and previous research (Clarke 1973) provide guidance on shear design under concentrated loads, either by a pyramid spatial strut-and-tie (ST) model or by extending a semi-empirical one-way bending theory-based design method to the two-way situation with a shear enhancement factor applied over a pile width. For wall loading, engineers employ the same rules, which is too conservative (Cao 2009). By commercial constraints in a design office, the real lower bound ST solution may never be found among multiple ST layout options. A commercial nonlinear numerical model (NNM), obtaining either ST topology or shear solution directly, may ill-converge at the paucity of test results for verification. Advanced NNM in research (e.g. Cao 2009) is more accurate but not economic for use in design practice.

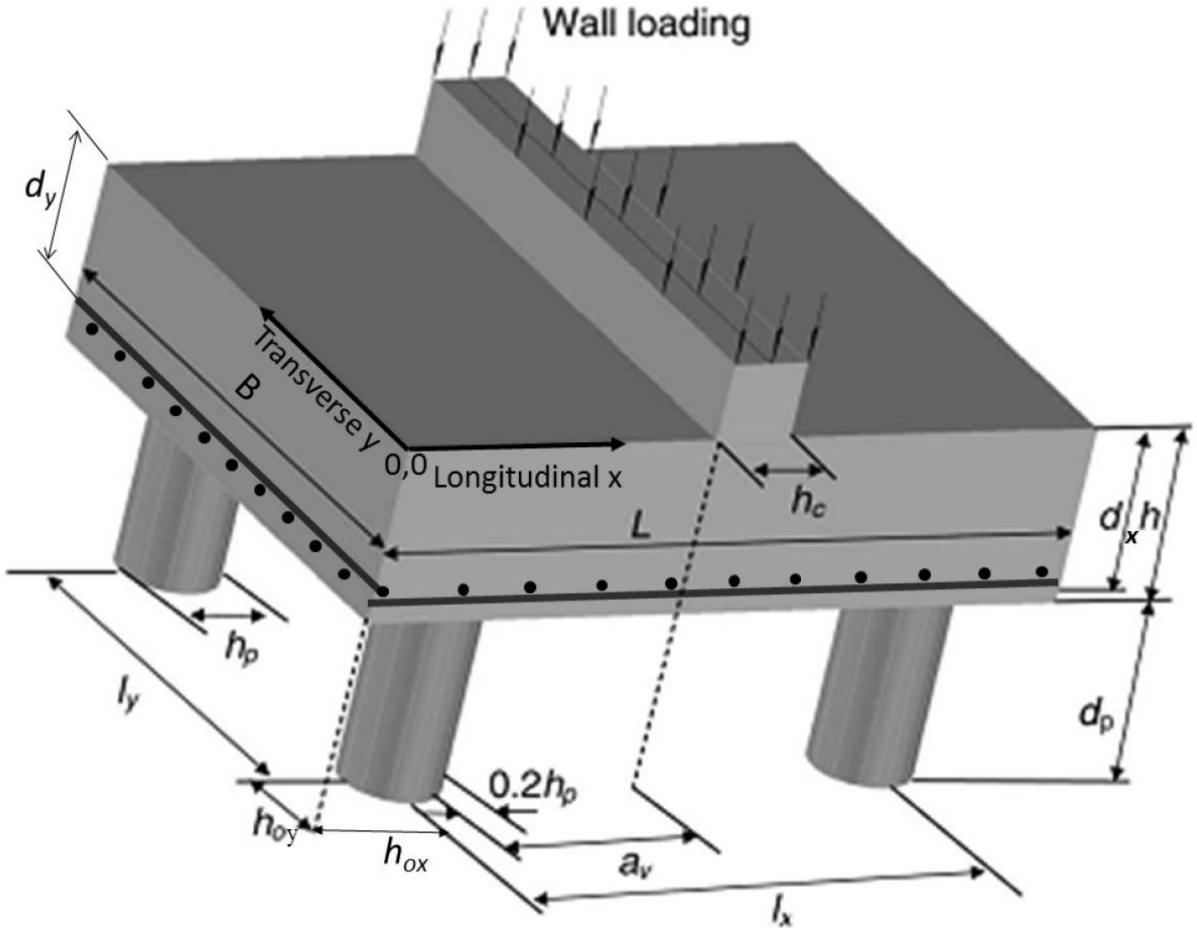


**Fig. 1.** Dimensions of a typical bridge RC four-pile cap under wall loading

The authors developed a semi-empirical ST model (Bloodworth et al. 2012; Cao 2009), verified against tests at UoS for caps over certain ranges of the geometric ratios n and μ (Table 1), which are respectively the LD and TD pile spacings ($l_x$, $l_y$) divided by pile diameter ($h_p$). An empirically derived 90% of the LD reinforcement $A_{st}$ was taken as the yielding tie, independent of $\mu$. Therefore, the model may not apply to cap configurations outside the test scope.

This research further develops a two-way grillage model representing true cap shear behaviour for general application. The model employs for the grillage elements a well verified linear constitutive relationship for simply supported one-way spanning RC deep beams. The grillage

**Table 1.** Key dimensions (mm) of pile cap samples at UoS (B4xx – experiment, E1xx parametrical study – only four extreme samples listed)

| Cap reference | Transverse direction (TD) | | | | Longitudinal direction (LD) | | | | | | Others | | | |
|---|---|---|---|---|---|---|---|---|---|---|---|---|---|---|
| | $l_y$ | $B$ | $d_y$ | $h_{oy}$ | $l_x$ | $L$ | $d_x$ | $h_{ox}$ | $h_c$ | $h_p$ | $h$ | $n=l_x/h_p$ | $\mu=l_y/h_p$ | $l_x/h$ | $l_y/h$ |
| B4A1 | 300 | 500 | 187 | 100 | 800 | 1100 | 199 | 150 | 100 | 130 | 230 | 6.15 | 2.31 | 3.45 | 1.30 |
| B4A2 | 300 | 500 | 187 | 100 | 650 | 950 | 199 | 150 | 100 | 130 | 230 | 5.00 | 2.31 | 2.86 | 1.30 |
| B4A3 | 300 | 500 | 187 | 100 | 550 | 850 | 199 | 150 | 100 | 130 | 230 | 4.23 | 2.31 | 2.38 | 1.30 |
| B4A4 | 300 | 500 | 187 | 100 | 500 | 800 | 199 | 150 | 100 | 130 | 230 | 3.85 | 2.31 | 2.17 | 1.30 |
| B4A5 | 300 | 500 | 187 | 100 | 400 | 700 | 199 | 150 | 100 | 130 | 230 | 3.08 | 2.31 | 1.72 | 1.30 |
| B4B1 | 300 | 500 | 190 | 100 | 650 | 950 | 200 | 150 | 100 | 130 | 230 | 5.00 | 2.31 | 2.86 | 1.30 |
| B4B2 | 450 | 650 | 190 | 100 | 650 | 950 | 200 | 150 | 100 | 130 | 230 | 5.00 | 3.46 | 2.86 | 1.96 |
| B4B3 | 550 | 750 | 190 | 100 | 650 | 950 | 200 | 150 | 100 | 130 | 230 | 5.00 | 4.23 | 2.86 | 2.38 |
| B4B4 | 700 | 900 | 190 | 100 | 650 | 950 | 200 | 150 | 100 | 130 | 230 | 5.00 | 5.38 | 2.86 | 3.03 |
| E1dl | 1200 | 1400 | 187 | 100 | 300 | 600 | 199 | 150 | 100 | 130 | 230 | 2.31 | 9.23 | 1.30 | 5.26 |
| E1ll | 1200 | 1400 | 187 | 100 | 1200 | 1500 | 199 | 150 | 100 | 130 | 230 | 9.23 | 9.23 | 5.26 | 5.26 |
| E1da | 150 | 350 | 187 | 100 | 300 | 600 | 199 | 150 | 100 | 130 | 230 | 2.31 | 1.15 | 1.30 | 0.65 |
| E1la | 150 | 350 | 187 | 100 | 1200 | 1500 | 199 | 150 | 100 | 130 | 230 | 9.23 | 1.15 | 5.26 | 0.65 |

model predicts shear capacity, reinforcement stress distribution and cap deflection rapidly, assisted by a VBA Userform based design software.

**UoS experimental samples**

The UoS experiments tested nine half-scale four-pile cap specimens, of which Fig. 2 is an example. Cap series B4A1~B4A5 and B4B1~B4B4 covered the ranges $3.08<n<6.15$ and $2.31<\mu<5.38$ (Table 1). Height to span ratios range $1.72<l_x/h<3.45$ and $1.30<l_y/h<3.03$. B4A1~B4A5 were designed with constant $\mu$ (=2.31) but varying $n$. B4B1~B4B4, with lower reinforcement ratio, have constant $n$ (=5.0) but varying $\mu$. These experiments were studied by advanced NMM which was then applied in 88 numerical samples in a parametric study (Cao 2009), extending geometries to $2.31<n<9.23$, $1.15<\mu<9.23$, $1.30< l_x/h<5.26$ and $0.65<l_y/h< 5.26$.

**Pile cap shear behaviour**

The proposed grillage model is developed to be compatible with the observed shear behavior:

1. Shear resistance develops both in LD and TD with major cracks running through front and back surfaces and minor bending cracks on the side surface extend into the soffit (e.g. Fig.2).
2. Reinforcement stress exhibits two-way behavior. LD stress (Fig.3) is constant at the yield stress $f_y$ (=547MPa) along the span for a strip along the front surface, degrading towards the cap centre. Fig. 4 shows high TD stress over the pile head on a width approximately $h_{ox} + l_x/4$.
3. The cap fails in a ductile LD ST mechanism, with tie width $h_{oy}+h_p/2$ width on each side.
4. Cap soffit deflection peaks at the cap centre and is zero at the pile heads.

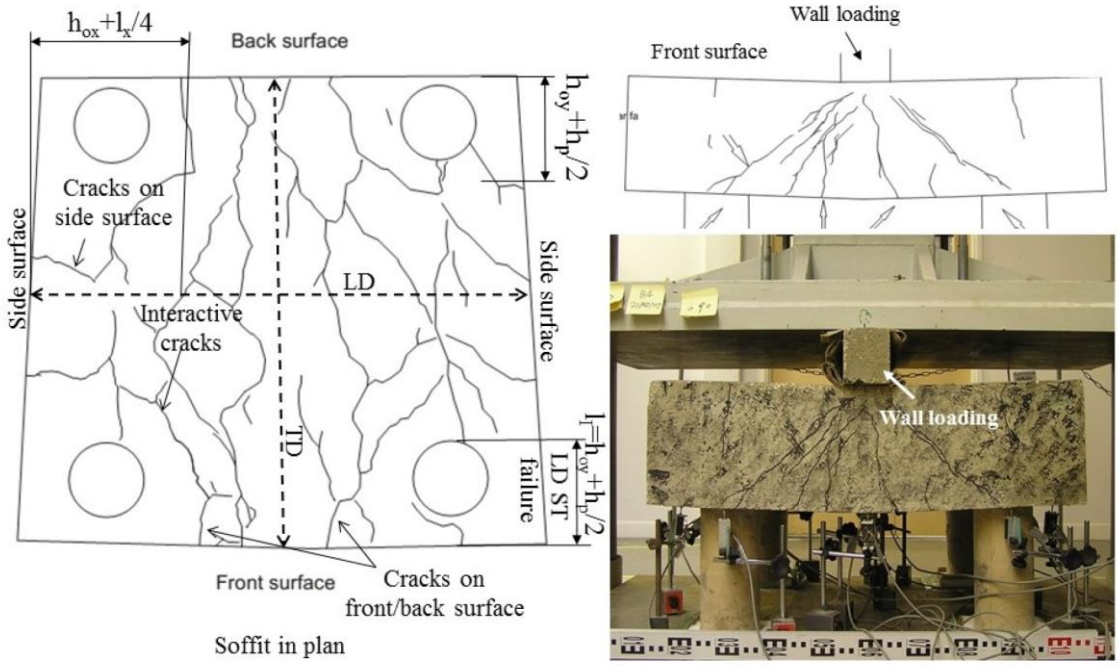


**Fig. 2.** Experimental observation of a UoS test sample at shear failure (B4B3 $n$=5.00, $\mu$=4.23)

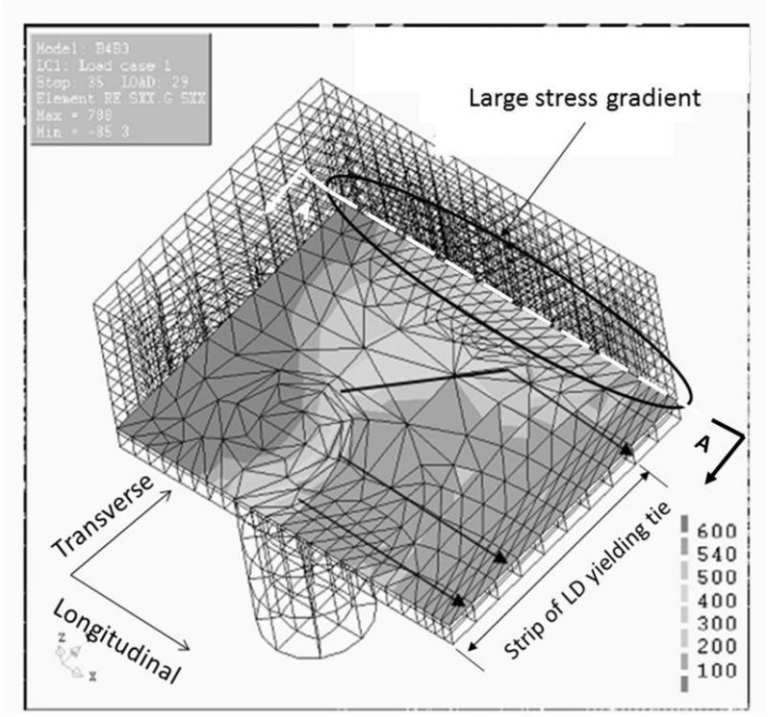


**Fig. 3.** Numerical model of ¼ pile cap showing LD reinforcement stress (MPa) at shear failure

(B4B3 $n$=5.00, $\mu$=4.23)

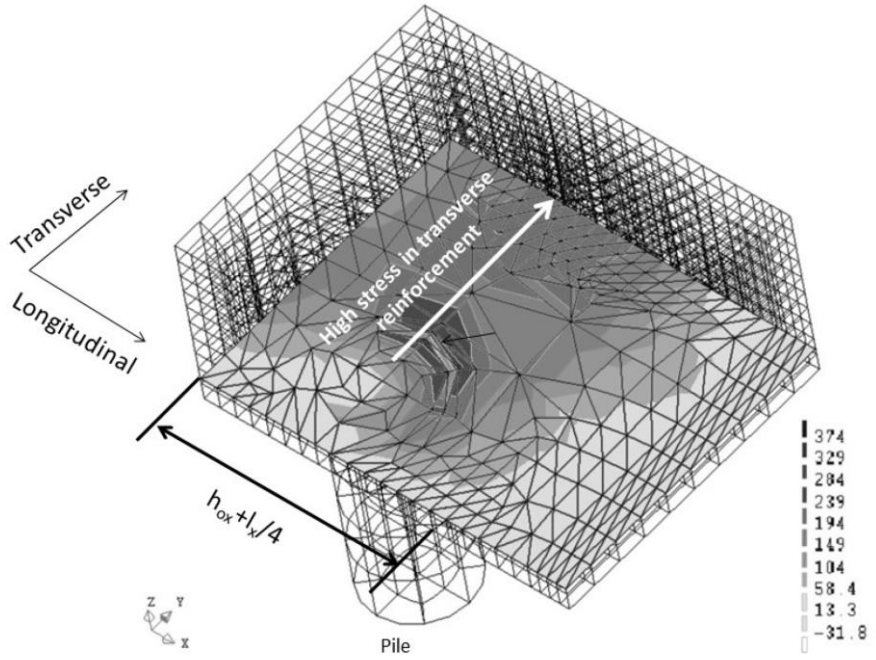


**Fig. 4.** Numerical model of ¼ pile cap showing TD reinforcement stress (MPa) at shear failure (B4B3 $n$=5.00, $\mu$=4.23)

**Proposed 2-way grillage model**

The 2-way cap shear behaviour leads to a grillage model with orthogonal elements of one-way RC deep beams, as shown in perspective view in Fig. 5 for a ¼ cap with side views in Figs. 6 and 7. The model consists of one front LD element of width $l_I$ spanning over the piles, a continuum of LD elements with infinitesimal width *dy* over width $l_{II}$ (see Fig. 7 for $l_I$ and $l_{II}$) and a TD element $n_1$-$n_0$-$n_{0'}$-$n_4$ with width $b_t$ (Fig. 6), bearing distributed transverse loading (*p(y)* in Fig.7) from the LD elements and transmitting shear to the front LD element at the pile inner edge through the point $n_{0'}$ of segment $n_1$-$n_0$-$n_{0'}$. This segment is assigned infinitely large bending and shear stiffness due to the short cantilever overhang. The resultant of p(y) is $P_{tAII}$, and similarly $P_{tAI}$ is the resultant of the force distributed over segment $n_1$-$n_0$-$n_{0'}$ (Fig. 7).

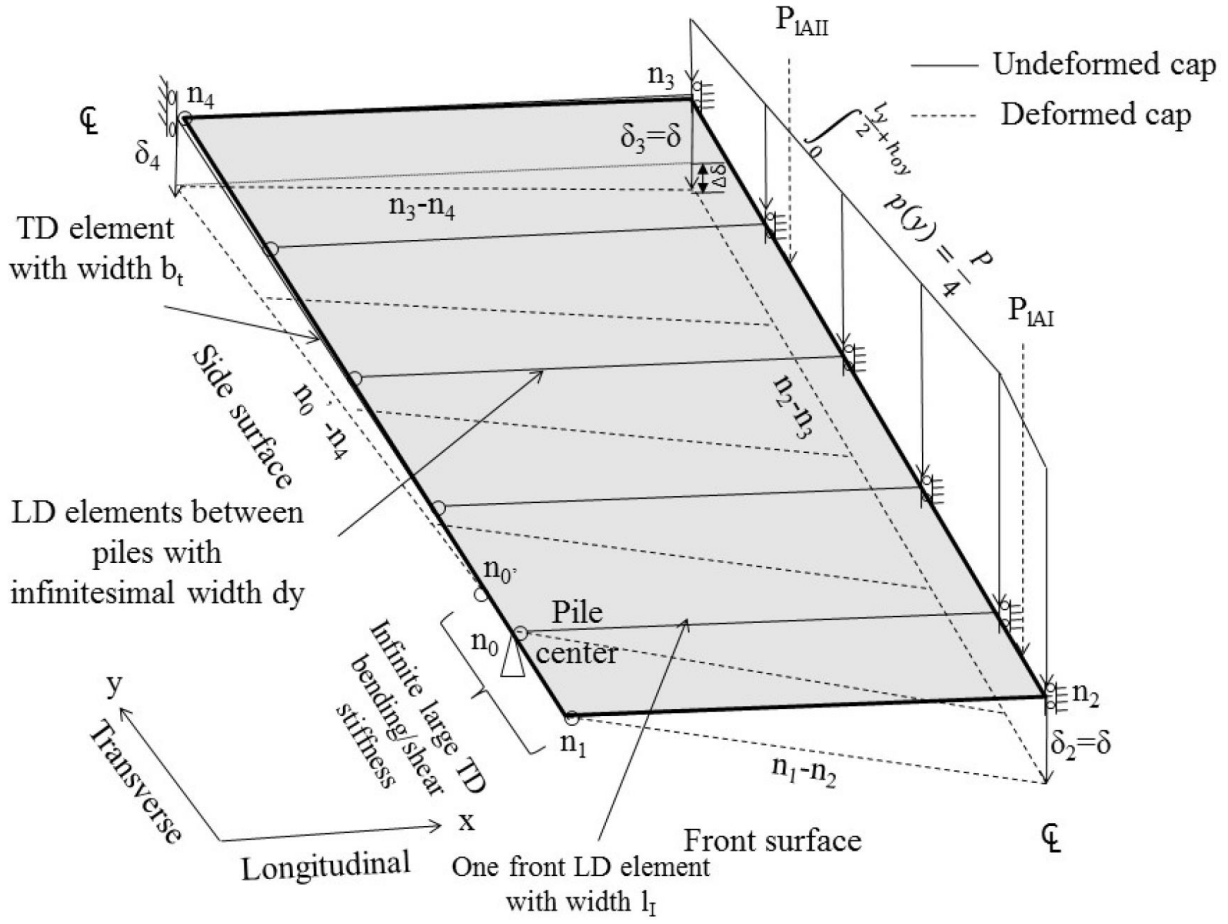


**Fig. 5**. Proposed grillage model for a ¼ pile cap under quarter of external load *P*

The model experiences uniform displacement under the wall loading (*i.e.* $\delta_2 = \delta_3 = \delta$ in Fig. 5) due to high in-plane bending stiffness of the loading wall, which complies with practice and test setups (Cao 2009). All elements are simply supported, deflecting linearly without shear interaction between adjacent vertical surfaces. For the total force in the TD reinforcement to be equal to that across cap length L/2 in reality, the proposed width of TD element $n_1$-$n_0$-$n_{0'}$-$n_4$, above which there is negligible shear capacity gain in the model, is: $b_t = h_{ox} + \frac{l_x}{4}$ (1)

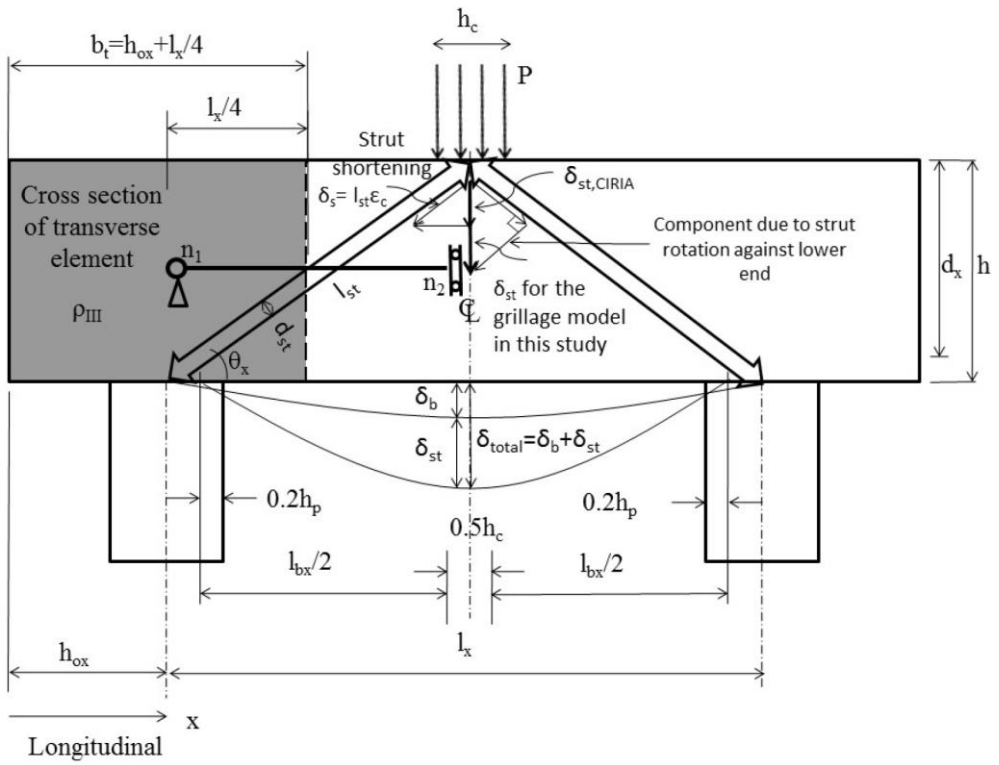


**Fig. 6.** Grillage elements and externally applied force seen from cap front surface

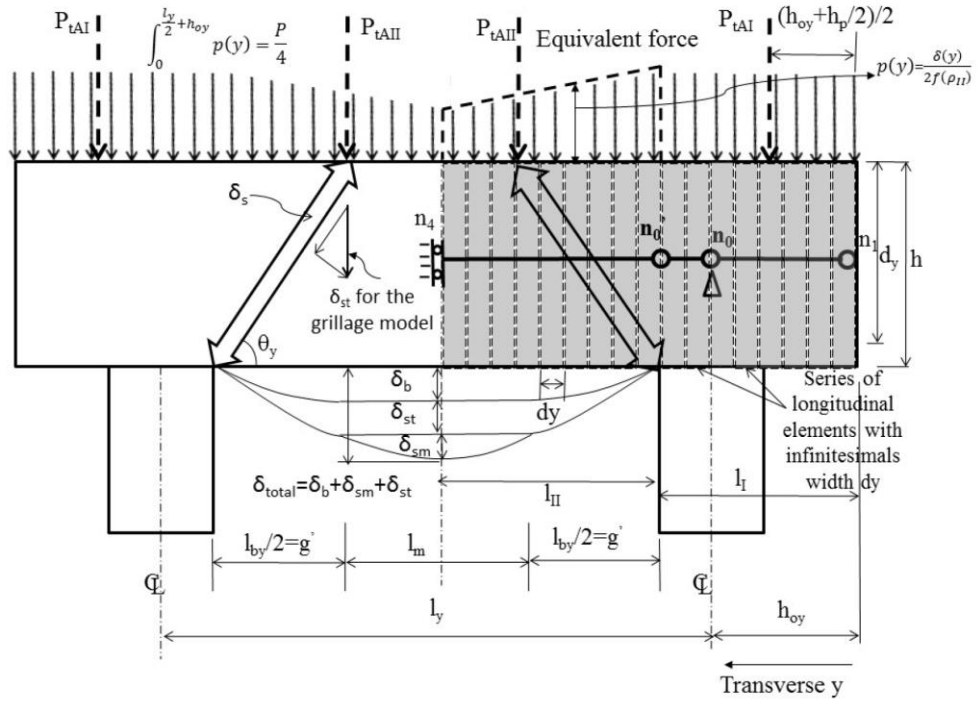


**Fig. 7.** Grillage elements and forces to TD elements seen from cap side surface

**Boundary conditions**

In Fig. 5, the boundaries $n_2$-$n_3$ and $n_3$-$n_4$ are assigned with full moment restraints in the vertical planes but with vertical shear released. The model is loaded along $n_2$-$n_3$ with a loading intensity $p(y)$ which integrates to $P/4$, where $P$ is the total load on the cap.

**Geometric compatibility**

Fig. 5 shows the cap boundaries $n_1$-$n_2$, $n_2$-$n_3$, $n_3$-$n_4$ and $n_{0'}$-$n_4$ deflect to dashed lines under the action of $p(y)$, with constant displacement along $n_2$-$n_3$ denoted as $\delta_2=\delta_3=\delta$. Deflection at $n_4$ is denoted as $\delta_4$ and $n_1$-$n_0$-$n_{0'}$ considered rigid as discussed earlier. Fig. 8 defines the angle $\alpha$ between the deformed $n_1$-$n_2$ and $n_3$-$n_4$. Due to $\alpha$ and angle between $n_1$-$n_2$ and the undeformed cap soffit both being small, $\delta_4$ can be expressed as: $\delta_4 = \frac{l_x}{2} \times \alpha$ (2)

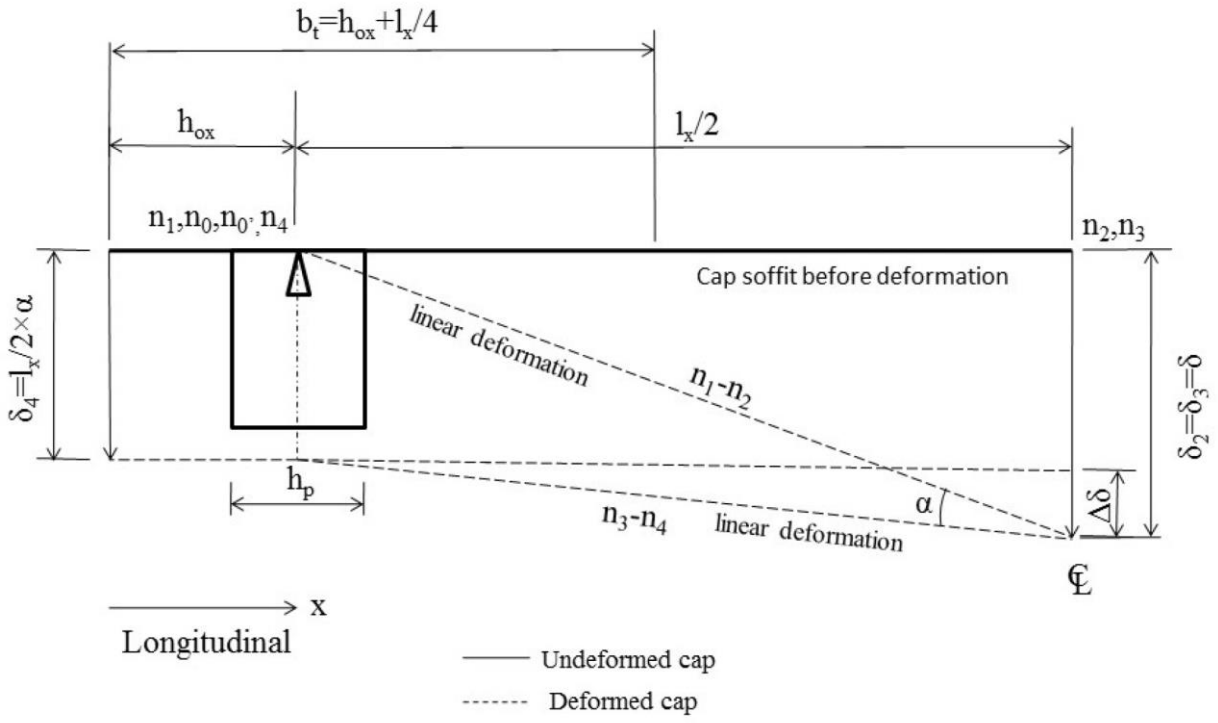


**Fig. 8.** Grillage deflection projected to the cap front surface

The relative deflection between $n_3$ and $n_4$ is $\Delta\delta$ (also in Figs. 5). Figs 9 and 10 show the soffit deflection seen from the side surface for two cases: $\delta_4>\delta$ (generally true for large $\mu$ with small $n$), and $\delta_4\leq\delta$ (for small $\mu$). The shaded area enclosed by deformed $n_2$-$n_3$, deformed $n_{0'}$-$n_4$ and undeformed rigid $n_1$-$n_0$-$n_{0'}$ represents the relative deflection of the LD elements. For larger $\mu$, $\delta_4$ tends to be larger than $\delta$, and the corresponding deformed $n_{0'}$-$n_4$ is shown in Fig. 9. This situation is impractical since it implies upward curvature in simply supported LD elements under downward external loading. The study shows that it is logical to set $\Delta\delta$=0 (i.e. $\delta_4=\delta$), where deformed $n_{0'}$-$n_4$ and $n_2$-$n_3$ encloses a triangle, i.e. $\Delta\delta = 0$ for $\delta_4 > \delta$. (3)

Considering Eq. 2, we also have: $\Delta\delta = \delta - \delta_4 = \delta - \frac{l_x}{2}\times\alpha$ for $\delta_4 \leq \delta$ (4)

The shaded area in Figs. 9 and 10 can be divided into area $A_{\text{I}}$ over $l_{\text{I}}$ and area $A_{\text{II}}$ over $l_{\text{II}}$, where:

$$l_I = \frac{h_p}{2} + h_{oy} \quad (5)$$

$$l_{II} = \frac{l_y}{2} - \frac{h_p}{2} \quad (6)$$

$$A_I = l_I \times \delta = (\frac{h_p}{2} + h_{oy}) \times \delta \quad (7)$$

Employing a deflection function $\delta(y)$ over axis $y$, $A_{II} = \int_{l_{II}} \delta(y)dy$ (8)

Where $dy$ is the infinitesimal width of LD elements (Fig.7).

If $\delta_4 > \delta$, considering Eqs. 3 and 6 and integrating Eq. 8, $A_{II} = \frac{\delta}{2} l_{II} = \frac{\delta}{2}\left(\frac{l_y}{2} - \frac{h_p}{2}\right)$ (9)

The centroidal distance to pile inner edge (Fig. 9), $g = \frac{l_{II}}{3} = \frac{\frac{l_y}{2}-\frac{h_p}{2}}{3}$ (10)

If $\delta_4 \leq \delta$, considering Eqs. 4 and 6, $A_{II} = \frac{\delta+\Delta\delta}{2} l_{II} = \frac{4\delta - l_x\alpha}{4}\left(\frac{l_y}{2} - \frac{h_p}{2}\right)$ (11)

The centroidal distance to pile inner edge (Fig. 10), $g = \frac{\frac{\delta\times l_{II}^2}{2}-\frac{\delta_4\times l_{II}^2}{3}}{A_{II}} = \frac{6\delta - 2l_x\alpha}{12\delta - 3l_x\alpha}\left(\frac{l_y}{2} - \frac{h_p}{2}\right)$ (12)

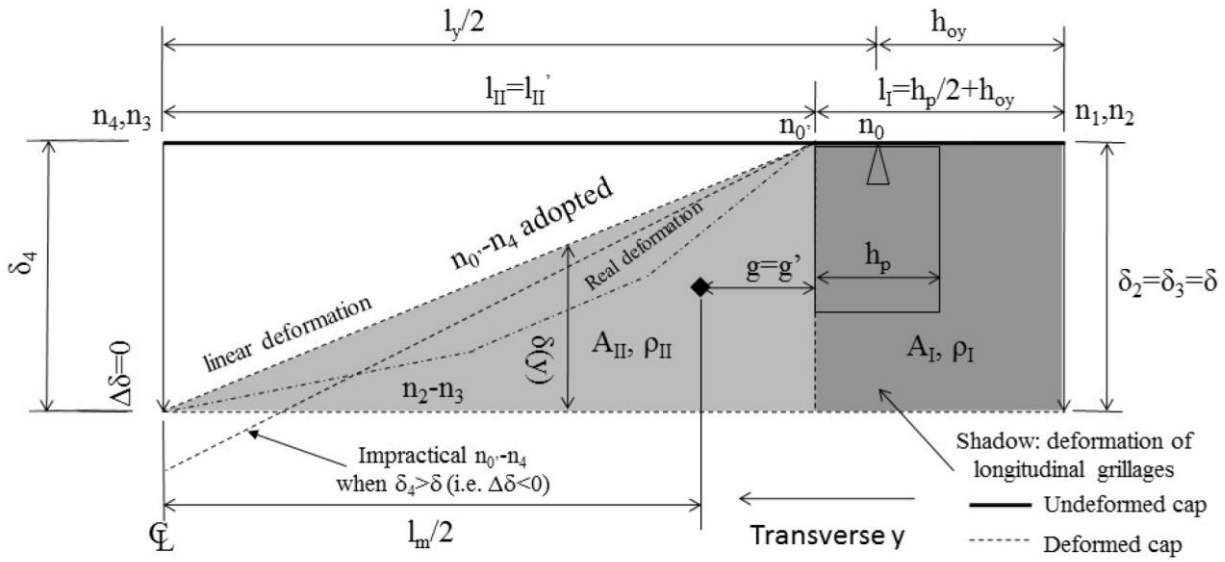


**Fig. 9.** Grillage deflection projected to cap side surface ($\delta_4 > \delta$)

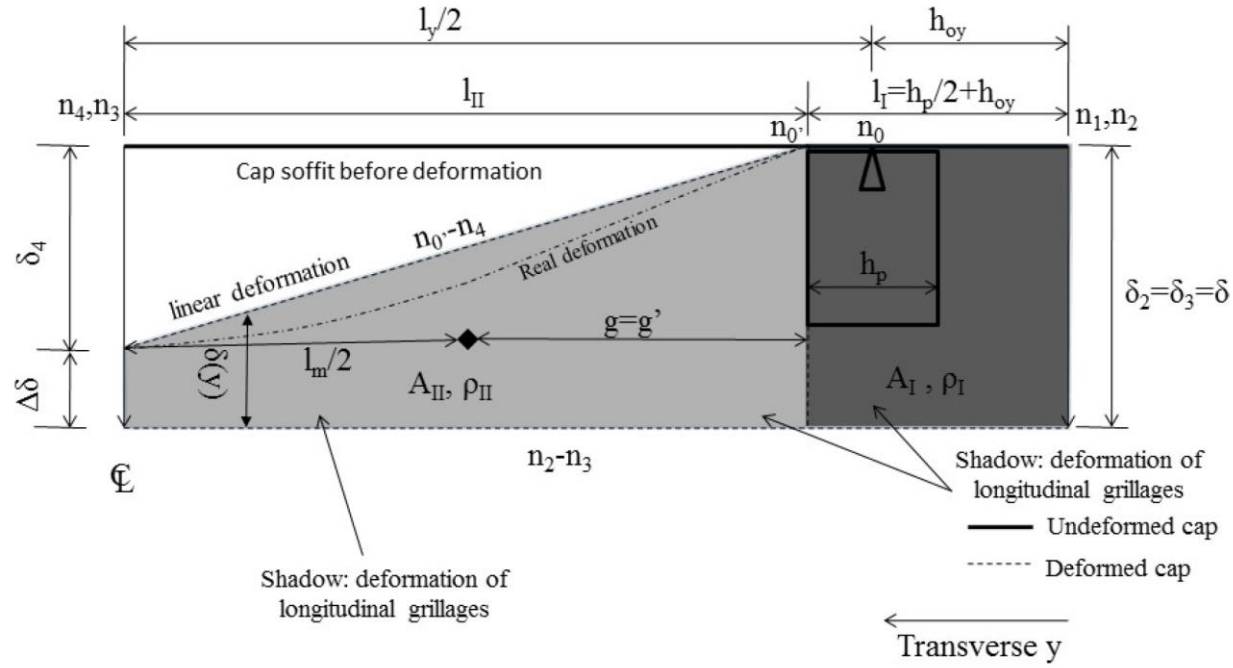


**Fig. 10** Grillage deflection projected to cap side surface ($\delta_4 \leq \delta$)

**Development of constitutive relationship for one-way RC deep beams**

A linear constitutive load-deflection relationship for the grillage elements is developed to solve the model efficiently. Evidence has it (Cao 2009) that shear resistance of RC deep beams is contributed from both flexural and ST behaviour, with the latter dominating at shear failure. Kani (1964) shows for three-point loaded (3PL) beams, a transition in strain distribution over the beam height along shear cracks from triangular (signifying bending) to uniform at ST failure. A procedure (CIRIA 1977) for predicting deflection of deep beams with $l_x/h < 2.0$ under 3PL assumes the deflection arises from reinforcement strain due to bending prior to cracking and a vertical component of concrete strut shortening $\delta_s$ (Fig. 6), plus downward movement of strut tips rotating to the geometric compatibility with reinforcement elongation.

Based on kinematic behaviour of RC deep beams observed in shear tests, Mihaylov et al. (2013, 2015) derived full load-deflection curves from four shear mechanisms (namely in critical loading zone, cracks interlock, stirrup, dowel action) and one flexural mechanism ('fan' shape rigid beam under the critical shear crack).

In light of these studies, a linear constitutive relationship is established by considering the summation of both bending and ST mechanisms acting in series, under the same external load P. For example, Fig. 6 is the 3PL scenario for UoS pile caps B4A1-B4A5 and B4B1 – close to one-way structures with small $l_y$. Total deflection $\delta_{total} = \delta_b + \delta_{st}$ under external loading $P$, where $\delta_b$ is Bernoulli beam theory based deflection. $\delta_{st}$ is the resultant of strut shortening $\delta_s$ and a component due to rotation of the strut around its lower end. Derivation of the term for $\delta_{st}$ is given in Appendix 1, from which it follows that:

$$\delta_{total} = (\frac{l_b^3}{48\times E_c\times I_{ef}} + \frac{\varepsilon_o^{'}\ \mathrm{h}}{2\sin\theta^2\tan\theta}\times\frac{1}{A_{st}f_y})P \quad (13)$$

The derivation of the second term of Eq. (13) is presented in Appendix 1.

The deflection at ST failure is derived by replacing P with shear capacity $P^*$, i.e.

$$P^* = 2A_{st}\,f_y\tan\theta \quad (14)$$

Where $\varepsilon_0^{'}$ is the concrete cylinder strain at peak strength $f_c^{'}$, ranging from 0.002 to 0.0025 for 15 MPa ≤ $f_c^{'}$≤ 50 MPa (Waner et al. 1998; BSI 2010). $\varepsilon_0^{'}$ = 0.002 is adopted here (Table 2). $E_c$ is concrete Young's modulus; $l_b$ is effective beam span (double the shear span measured from the external loading positions); $\vartheta$ is strut angle; $h$ is beam depth; $A_{st}$ is area of LD reinforcement; $f_y$ is reinforcement yield strength. Effective second moment of area for a deep beam, $I_{ef}$ is given by (Standards Australia 2004) as $I_{ef}(\rho, d) = Y(\rho, d)B$ (15)

**Table 2.** Key material properties of pile cap samples at UoS (B4xx - experiment, E1xx parametrical study – only four extreme samples listed)

| Cap reference | Concrete | | | | Reinforcement | | | |
|---|---|---|---|---|---|---|---|---|
| | $f_{cu}$ (MPa) | $f_c'$ (MPa) | $\varepsilon_o'$ | $E_c$ (GPa) | $f_y$ (MPa) | $E_s$ (GPa) | $\rho_I = \rho_{II}$ (%) | $\rho_{III}$ (%) |
| B4A1 | 20.3 | 16.24 | 0.002 | 25.3 | 547 | 210 | 1.137 | 1.210 |
| B4A2 | 21.8 | 17.44 | 0.002 | 25.8 | 547 | 210 | 1.137 | 1.210 |
| B4A3 | 24.3 | 19.44 | 0.002 | 26.7 | 547 | 210 | 1.137 | 1.210 |
| B4A4 | 24.4 | 19.52 | 0.002 | 27.1 | 547 | 210 | 1.137 | 1.210 |
| B4A5 | 23.0 | 18.40 | 0.002 | 26.2 | 547 | 210 | 1.137 | 1.210 |
| B4B1 | 19.5 | 15.60 | 0.002 | 24.8 | 547 | 210 | 0.786 | 0.827 |
| B4B2 | 25.6 | 20.60 | 0.002 | 27.3 | 547 | 210 | 0.786 | 0.827 |
| B4B3 | 24.7 | 19.76 | 0.002 | 27.0 | 547 | 210 | 0.786 | 0.827 |
| B4B4 | 21.0 | 16.80 | 0.002 | 25.7 | 547 | 210 | 0.786 | 0.827 |
| E1dl | 25.0 | 20.00 | 0.002 | 28.0 | 547 | 210 | 1.137 | 1.137 |
| E1ll | 25.0 | 20.00 | 0.002 | 28.0 | 547 | 210 | 1.137 | 1.137 |
| E1da | 25.0 | 20.00 | 0.002 | 28.0 | 547 | 210 | 1.137 | 1.137 |
| E1la | 25.0 | 20.00 | 0.002 | 28.0 | 547 | 210 | 1.137 | 1.137 |

Where $Y(\rho,d)=(0.02+0.025\rho)d^3$ when $\rho \geq 0.005$ and $Y(\rho,d)=(0.1-0.135\rho)d^3 \geq 0.06d^3$ when $\rho < 0.005$, and *B* is the beam width.

For four-point loading (4PL), e.g. for the TD element between piles shown in Fig. 7 with two pointed loads $P_{tAll}$ distanced at spacing $l_m$, $\delta_{total} = \delta_b + \delta_{st} + \delta_{sm}$, where $\delta_{sm}$ is the deflection of the intermediate beam segment $l_m$ subject to uniform bending moment only. Thus:

$$\delta_{total}=\left(\frac{l_b^3}{48\times E_c\times I_{ef}}+\frac{\varepsilon_o' \, h}{2\sin\theta^2\tan\theta}\times\frac{1}{A_{st}f_y}+\frac{l_b l_m^2}{32\times E_c\times I_{cr}}\right)P \qquad (16)$$

Where $I_{cr}$ is the beam cracked second moment of area.

**Validation of the proposed constitutive relationship**

A comparison between Eqs. (13) and (14) with experiment is shown in Fig. 11 for UoS cap B4A3, which gives good match for stiffness, kink point and ultimate load.

Combined with UoS tests, deflections at SLS load level round 70% of $P^*$ (Fig. 11) in a series of international tests (Rao et al. 2007; Kotsovos 1987; Yang and Jun 2003; De Paiva and Austin 1960) on caps under a mixture of 3PL, 4PL and uniformly distributed load (equivalent to 4PL) were compared with Eqs.(13) and (16). The comparison (Fig. 12) shows good match between measured and predicted deflections, which are slightly conservative for both equations.

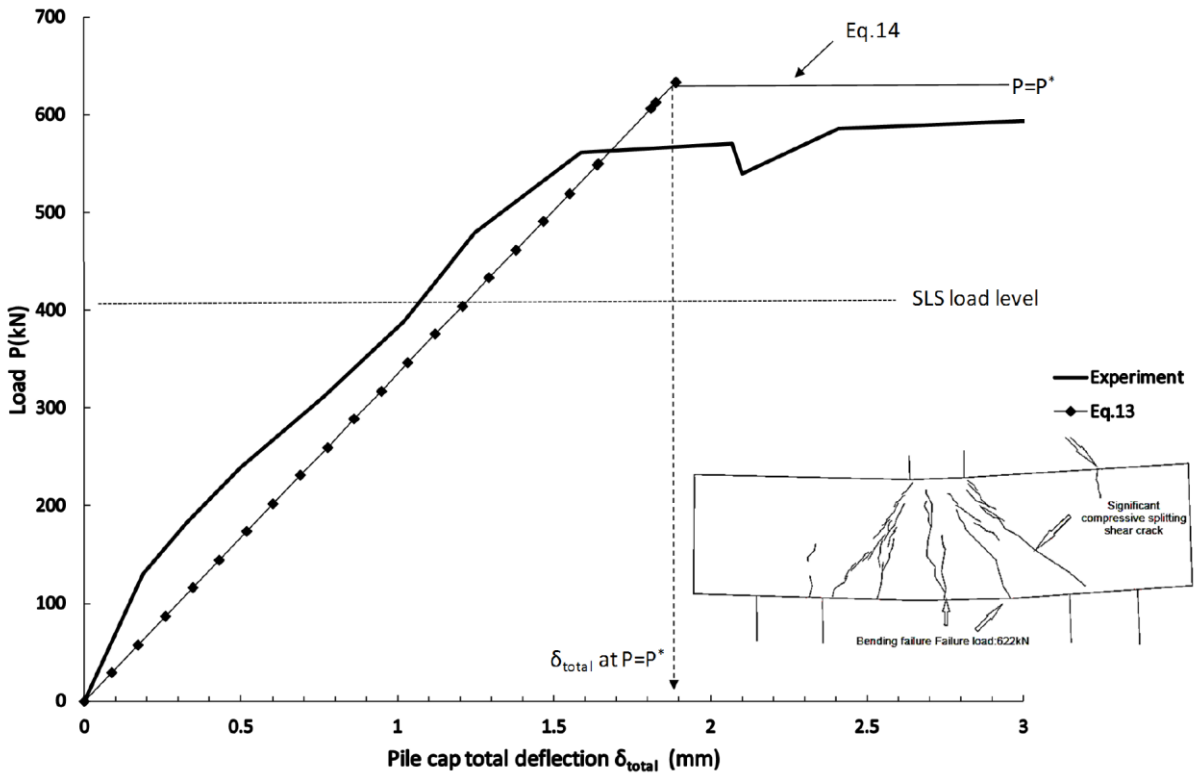


**Fig. 11** Load-deflection relationship for 3PL UoS pile cap B4A3 ($n$=4.23, $\mu$=2.31)

**Application of constitutive relationship to LD grillage elements**

As LD grillage elements (Figs. 5 and 6) are subject to 3PL, Eq. (13) applies. Taking the shear span between lines at 20% of pile diameter from the inner edge (BSI 1990):

$$l_b = l_{bx} = l_x - 2 \times 0.3 \times h_p - \frac{h_c}{2} \qquad (17)$$

Taking the shear span as $l_b$ rather than the pile centre span $l_x$ in Eq. (17) compensates for the reality that there will be some hogging moment restraint to the cap from the piles to the cap so that the imagined grillage elements are not truly simply supported. An elastic frame analysis (Cao 2009) showed that reducing the shear span in this way was in close agreement with Eq. (17). It was also observed in UoS experiments that although hogging vertical cracks above the piles propagated under early loading when behavior was predominantly bending, they stabilized

during maturing of the ST mechanism in the failure stage (Cao 2009). Therefore, this simplification to simply supported conditions but with reduced shear span $l_b$ is thought to be sufficiently accurate for practical pile caps.

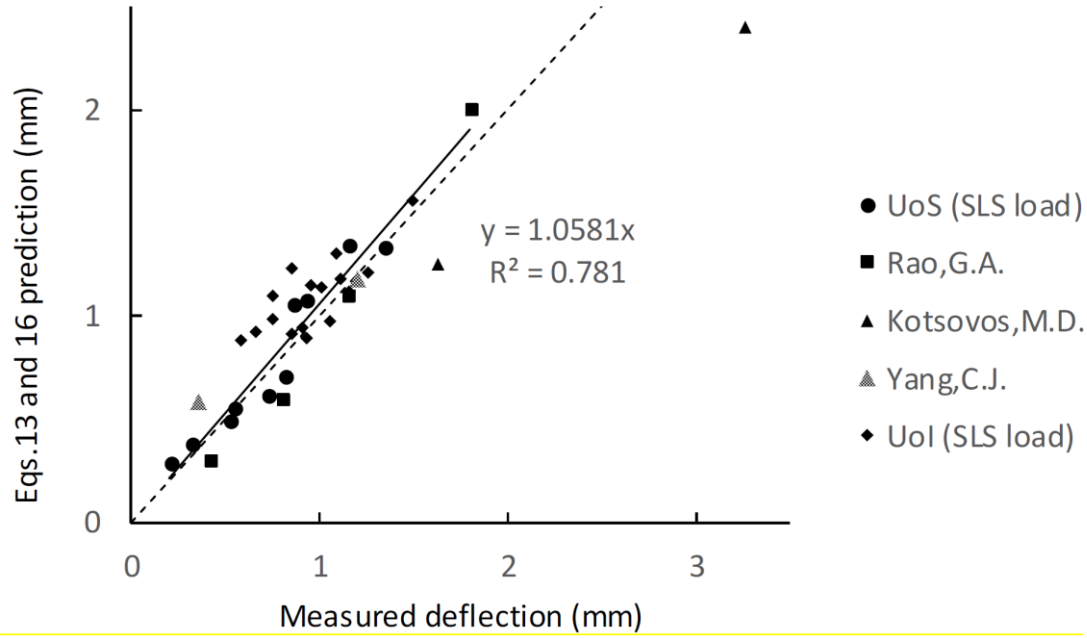


**Fig.12** Comparison between Eqs. 13 and 16 predictions and measured deflections at SLS load for all samples in the study

Concrete strut angle for LD elements is: $\theta_x = \tan^{-1}\frac{h}{\frac{l_x}{2}}$ (18)

An LD element of width *dy* is subjected to external loading (Fig. 5) $P = 2p(y)dy$ (19)

From Eq.(13), define $f(\rho_I)$ and $f(\rho_{II})$ as LD element flexibility over the lengths $l_I$ and $l_{II}$, respectively:

$$f(\rho_I) = \frac{l_{bx}^3}{48\times E_c \times Y(\rho_I, d_x)} + \frac{\varepsilon_o' h}{2\sin\theta_x{}^2 \tan\theta_x} \times \frac{1}{\rho_I d_x f_y} \quad (20)$$

$$f(\rho_{II}) = \frac{l_{bx}^3}{48\times E_c \times Y(\rho_{II}, d_x)} + \frac{\varepsilon_o' h}{2\sin\theta_x{}^2 \tan\theta_x} \times \frac{1}{\rho_{II} d_x f_y} \quad (21)$$

Where $\rho_I$, $\rho_{II}$ are the reinforcement ratios (Table 2) and $d_x$ the effective LD beam depth (Table 1).

From Figs. 9~10, $\delta_{total}$ for LD elements over width $l_I$ is equal to $\delta(y)=\delta$ and over width $l_{II}$ is equal to $\delta(y)$. Substituting Eqs. (19)-(21) into Eq. (13) and integrating along $y$:

Over $l_I$: $\int_{l_I} \delta(y)dy = A_I = \int_{l_I} f(\rho_I)2p(y)dy = 2f(\rho_I)\int_{l_I} p(y)dy = 2f(\rho_I)\mathrm{P}_{lAI}$ (22)

Over $l_{II}$: $\int_{l_{II}} \delta(y)dy = A_{II} = \int_{l_{II}} f(\rho_{II})2p(y)dy = 2f(\rho_{II})\int_{l_{II}} p(y)dy = 2f(\rho_{II})\mathrm{P}_{lAII}$ (23)

Where $P_{lAI}$ and $P_{lAII}$ are the resultant external loading applied to the LD elements on the quarter cap over the lengths $l_I$ and $l_{II}$ respectively (Fig. 5).

**Application of Constitutive relationship for TD grillage elements**

For the TD element, Eq. (16) applies, in which $l_m$ (Fig. 7) is the intermediate beam length between resultant loads $P_{tAII}$ transferred from LD elements. Effective span $l_b = l_{by}$ for $n_0'$-$n_4$, twice the distance $g'$ measured from the inner edge of the pile to each $P_{tAII}$.

Eqs. (22) and (23) imply that the enclosed shapes of $p(y)$ and the deflection $\delta(y)$ have the same horizontal length but with vertical heights similar by scale factors $2f(\rho_I)$ and $2f(\rho_{II})$. For example, the trapezoidal area enclosed by dashed lines in Fig. 7 has the same length $l_{II}$ as area $A_{II}$ in Fig. 10 but height $p(y)$ scaled by $2f(\rho_{II})$ from δ(y) in Fig.10, i.e. $p(y) = \frac{\delta(y)}{2f(\rho_{II})}$. Therefore, distances to centroids $g'$=$g$ (with $g$ from Eqs. (11) and (12)). Thereby, $l_{by} = 2g' = 2g$ (24)

Substituting into Eq. (16) with $l_b = l_{by}$, $l_m = l_y - h_p - 2g$, $b = b_t$, $d = dy$, $\vartheta = \vartheta_y$, $\rho = \rho_{III}$, $\delta_{total} = \delta_4$ and $P$=2$P_{tAII}$, defines the TD element flexibility $f(\rho_{III})$ as:

$$f(\rho_{III}) = \frac{l_{by}^3}{48\times E_c \times Y(\rho_{III},d_y)b_t} + \frac{\varepsilon_o' h}{2\,sin\theta_y{}^2\,tan\,\theta_y} \times \frac{1}{\rho_{III} d_y b_t f_y} + \frac{l_b(l_y-h_p-2g)^2}{32\times E_c \times Y(\rho_{III},d_y)b_t} \quad (25)$$

Where: $\theta_y = tan^{-1}\frac{h}{g}$. Eq. (16) becomes: $\delta_4 = f(\rho_{III}) \times 2P_{tA_{II}}$ (26)

**Force equilibrium**

The external forces $P_{lA_I}$ and $P_{lA_{II}}$ applied to LD elements (Fig.5) are balanced by the reactions at the connection to the TD element, $P_{tA_I}$ and $P_{tA_{II}}$(Fig.7), which cause deflection in the TD element. Considering a quarter cap: $P_{lA_I} + P_{lA_{II}} = P_{tA_I} + P_{tA_{II}} = \frac{P}{4}$ (27)

**Failure criteria**

Failure is observed by ST failure in LD elements over transverse width $l_I$ above the piles (Fig. 2). Figs. 9-10 indicate that cap deflection $\delta$ along $l_I$ is always higher than $\delta(y)$ along $l_{II}$ in the model, ensuring shear failure along $l_I$ prior to $l_{II}$. It is also reflected in the grillage layout (Fig. 5) that once the front LD element fails, it is no longer capable of supporting the TD element over $n_{0'}$, leading immediately to overall structural failure. The corresponding deflection $\delta$ of the front LD element at failure can be obtained from Eqs. (13), (19) and (20) by replacing the general load intensity $p(y)$ with the load intensity at failure $p(y)^*$: $\delta = f(\rho_I) 2p(y)^*$ (28)

Considering the force balance with the tie reinforcement in the ST model, $p(y)^* \times dy = tan\,\theta_x \rho_I d_x f_y dy$ . Therefore, $p(y)^* = tan\,\theta_x \rho_I d_x f_y$ (29)

**Shear capacity**

Rearranging Eq. (23) gives: $\frac{A_{II}}{2f(\rho_{II})} = \int_{l_{II}} p(y)dy = P_{lA_{II}}$ (30)

$A_{II}$ is derived from Eqs. (9) or (11), in which $\delta$ can be obtained from Eq. (28). $P_{lAII}$ (= $P_{tAII}$ = $\frac{\delta_4}{2f(\rho_{III})}$) is obtained from Eq. (26), where $\delta_4$ is derived from Eq. (2). As a result, Eq. (30) contains only one unknown, namely $\alpha$ (*e.g.* $\alpha$ in Eq. (11) for $A_{II}$), the relative angle of soffit deflection between the

deformed $n_1$-$n_2$ and $n_3$-$n_4$ (Fig. 8). As Eq. (30) contains a complex nonlinear function of $\alpha$, a numerical solution is proposed. Re-organizing Eq. (30), function *f(α)* is defined as:

$$f(\alpha) = \frac{A_{II}}{2f(\rho_{II})} - \frac{\delta_4}{2f(\rho_{III})} \quad (31)$$

Following the procedure below, the solution for α is sought when *f(α)*=0:

1. Assume that $\delta_4 \leq \delta$ and substitute Eqs. (2), (11), (21)-(25) into Eq. (31) Trial values of $\alpha$ in increments between 0.00001~0.0001 radians, from which the *α-f(α)* curve is obtained.
2. The solution for α is obtained and the procedure stops when either:

(i) Two consecutive values of *f(α)* have opposite sign, when $\alpha < \frac{\delta}{\frac{l_x}{2}}$ (i.e. $\delta_4 < \delta$ as per Eq. 2), so obtain $\alpha$ for *f(α)*=0 by linear interpolation between the two neighboring points.

(ii) If $\alpha = \frac{\delta}{\frac{l_x}{2}}$ is reached prior to two consecutive f(α) values changing sign, the solution is $\alpha = \frac{\delta}{\frac{l_x}{2}}$ (i.e. $\delta_4 = \delta$). This normally only occurs for caps with particularly large $\mu$ and small $n$.

Fig. 13 shows a worked example for cap B4B4. Procedure 2(i) applies for this case, with $\alpha = 0.00108$ for $\delta_4 < \delta$ obtained. Having $\alpha$, $A_{II}$ is obtained from Eq. (11). Then derive $P_{lA_I}$ and $P_{lA_{II}}$ from Eqs. (22) and (23). Denoting $P$=$P^*$ as the external force at shear failure, *i.e*. the cap shear capacity, the expression for cap shear capacity, by transforming Eq. (27) becomes:

$$P^* = 4\left(\frac{A_{II}}{2f(\rho_{II})} + \frac{A_I}{2f(\rho_I)}\right) \quad (32)$$

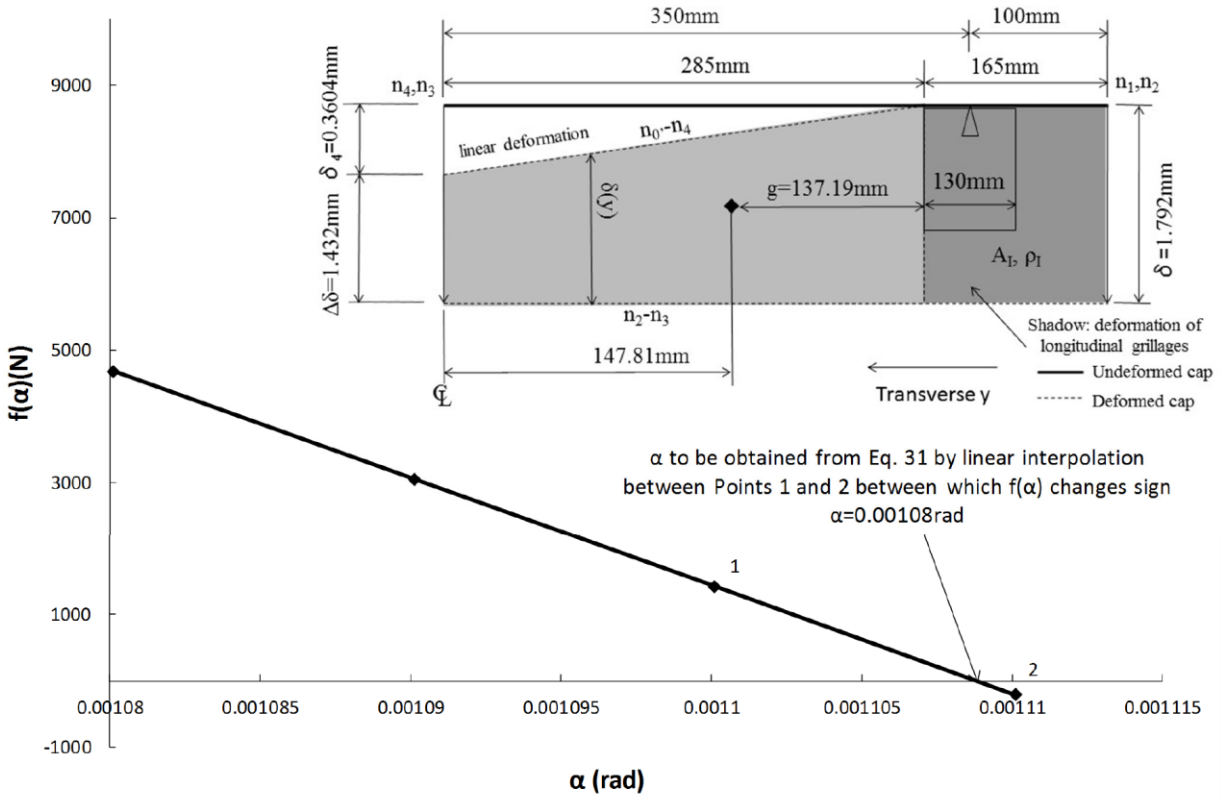


**Fig. 13** *α-f*(*α*) curve and solution for $\alpha$ for cap B4B4 (*n*=5.00, *μ*=5.38)

**Reinforcement stress and cap soffit deflection**

Reinforcement stress is obtained using the same philosophy, namely by linear superposition of the stresses from bending and ST mechanisms, but capped by the maximum achievable $f_y$. Soffit deflection at any location *δ(x,y)* is calculated by bi-linear interpolation between $\delta_4$, $\Delta\delta$ and $\delta$ obtained previously (Figs. 5 and 8).

**VBA Userform based design software S4PWv1.0**

The above procedure has been written into a VBA Userform based design software *S4PWv1.0* of which the user interface is shown in Fig. 14. It allows engineers to assign cap dimensions and

material properties. Running within 5 seconds for each case, the programme provides cap shear capacity, full field cap deflection and TD/LD reinforcement stress distribution (over a ¼ cap).

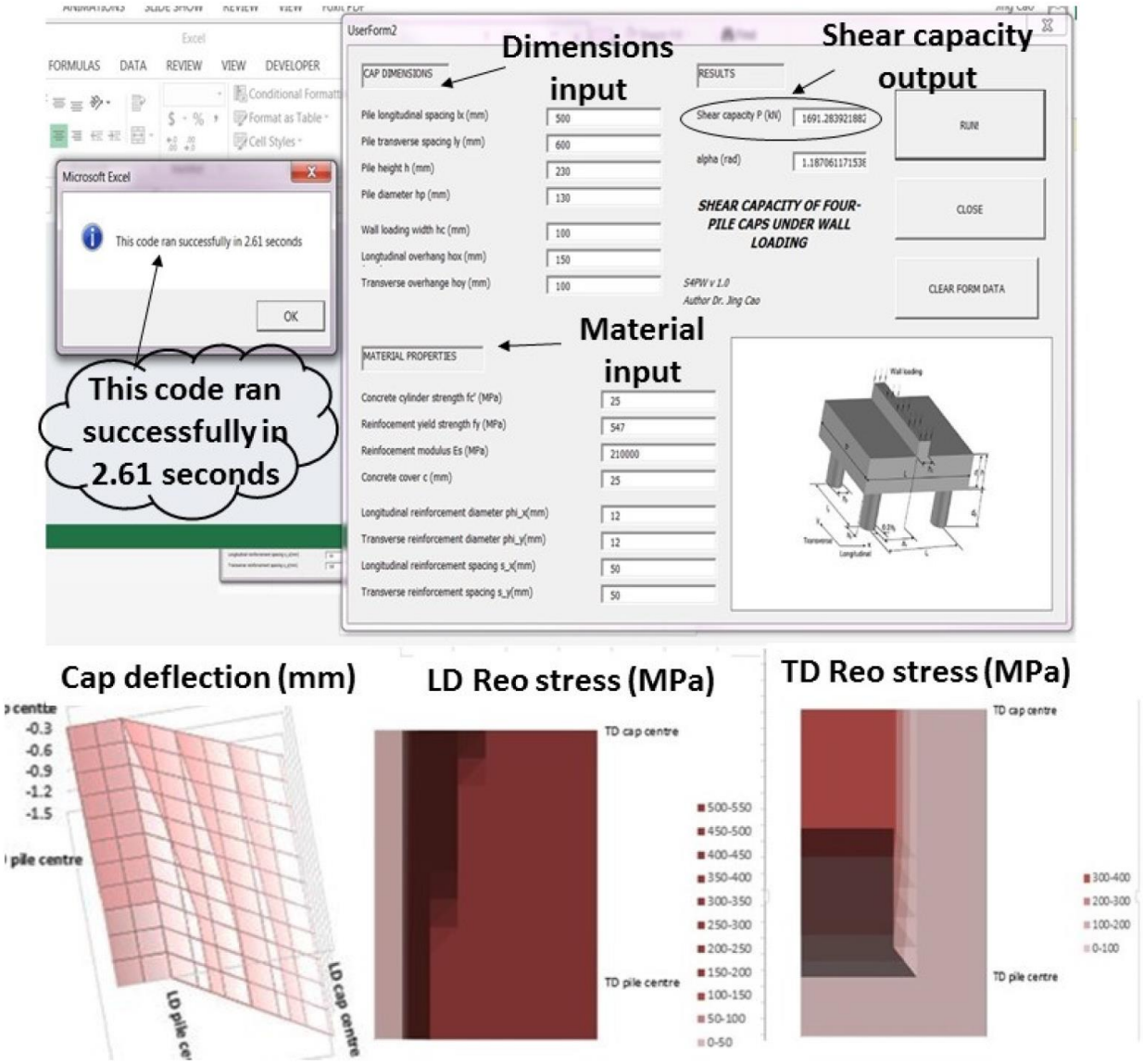


**Fig. 14** VBA Userform based design software *S4PWv1.0* for solving grillage model for bridge RC four-pile cap under wall loading

**Comparison for shear capacity**

The shear capacity predicted from Eq. (32) (calculated by *S4PWv1.0*) is compared with UoS experimental samples, NNM and four extreme numerical models from the parametric study

(refer Tables 1- 2). Fig. 15 shows the predictions match well with both the experimental results and numerical modeling. Due to the innate variability of experimental data, Eq. (32) shows higher accuracy and less scatter against NNM samples ($R^2$=0.9827) than against experimental samples ($R^2$=0.8597). Cap B4A5 failed by crushing of the piles, both in the experiment and NNM simulation, and B4A2 partially failed in the experiment towards the cap back surface (Cao 2009; Cao and Bloodworth 2012). The shear capacity of these two caps should have been higher, meaning Eq. (32) would perform even better. Excluding these two caps, the cumulative distribution function of the prediction error is shown in Fig. 15. The probability of exceedance of Eq. (32) compared to the experiment and NNM is 96% and 78% respectively, showing conservatism level of Eq. (32).

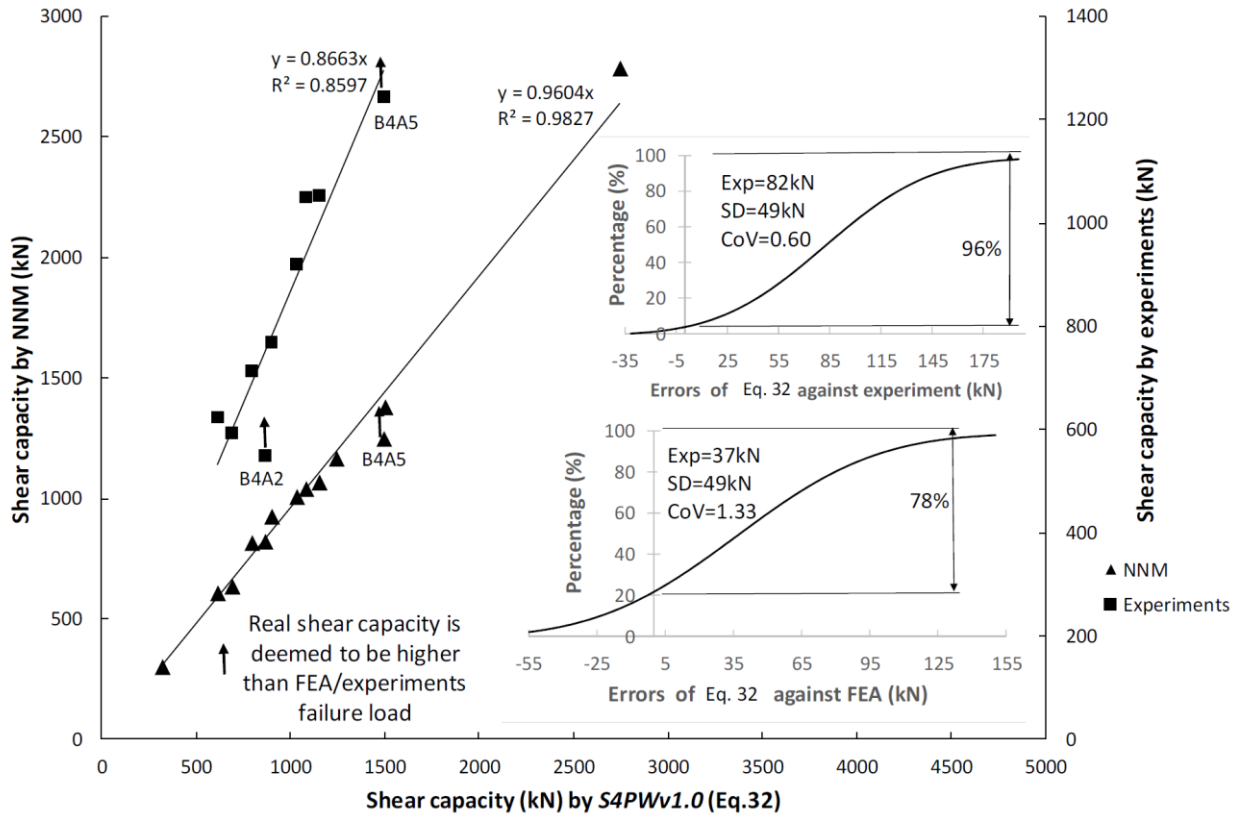


**Fig. 15** Comparison of shear capacity from *S4PWv1.0* with FEA and experiment samples

Fig.16 shows the comparison for shear capacity between Eq. (32) and NNM for all 88 parametric cap samples, from which good match is seen. Eq. (32) slightly underestimates the capacity, albeit high $R^2$=0.9684. The circled cases deviating from the group are individual caps with impractical dimensions of extreme large $l_y$. The shear capacity from NNM for experiment samples is also included which, if combined with parametric samples excluding impractical dimensions, makes Eq. (32) more faithful to NNM with $R^2$=0.9874. The probability of exceedance of Eq. (32) is 42%.

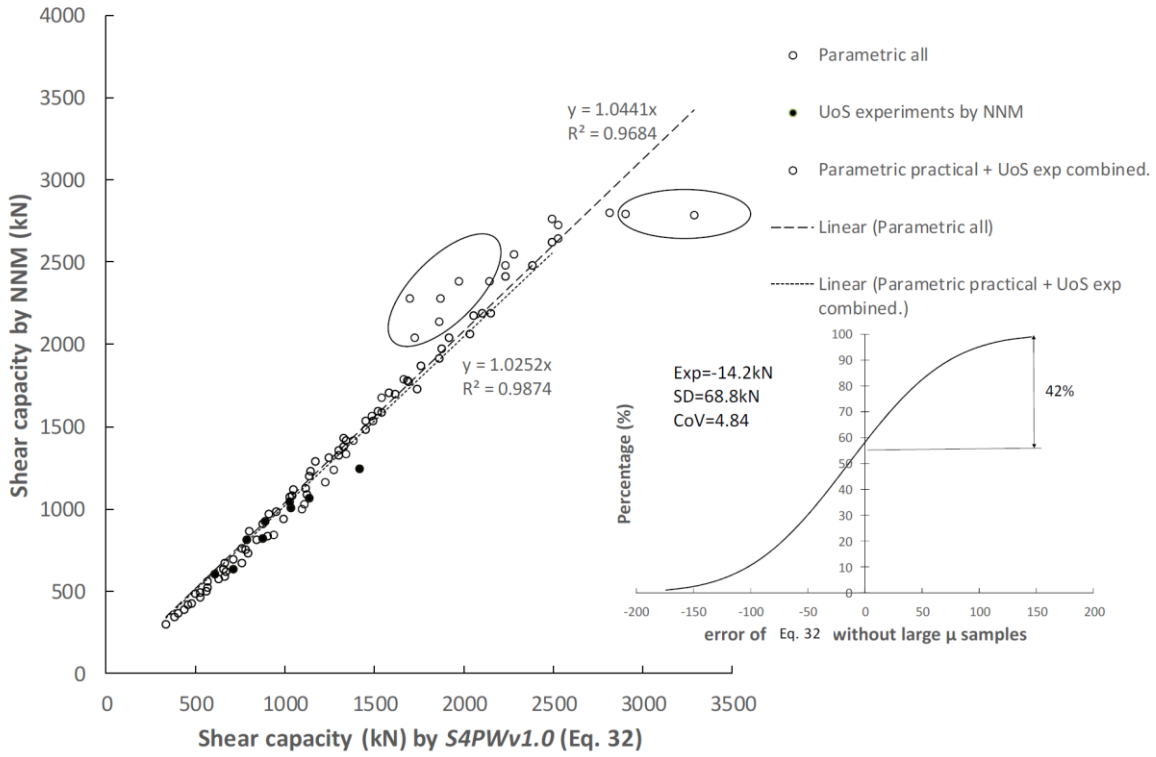


**Fig. 16** Comparison for shear capacity between *S4PWv1.0* and NNM of all parametric studies combined and experimental samples by FEA

**Comparison for reinforcement stress**

Comparison of LD reinforcement stress for cap B4B3 at shear failure from NNM and *S4PWv1.0* is shown in Figs. 3 and 17. Both figures show the yield strength $f_y$=547MPa is mobilized on the whole LD span over a certain strip width measured inwards from the cap front surface. Fig. 18 compares

LD reinforcement stress along A-A section in Figs. 3 and 17 between NNM and *S4PWv1.0,* both capturing the LD stress gradient along the TD centreline. NNM predicts 300MPa stress at $x=h_{ox}$ and 547MPa at midspan, while variation from 470MPa to 547MPa is estimated by S4PWv1.0. Reinforcement stress is also compared for the 88 parametric study numerical samples. For example, Fig. 19 shows comparison for full field LD reinforcement stress distributions between NNM and *S4PWv1.0* on ¼ cap E1dl, where similar distributions can be seen. The stress along A-A is compared in Fig. 20. $f_y$=547MPa is reached in both methods, with the plateau in each extending to 330mm from the cap front surface (y=0mm), followed by stress degradation of similar magnitude towards the cap centre.

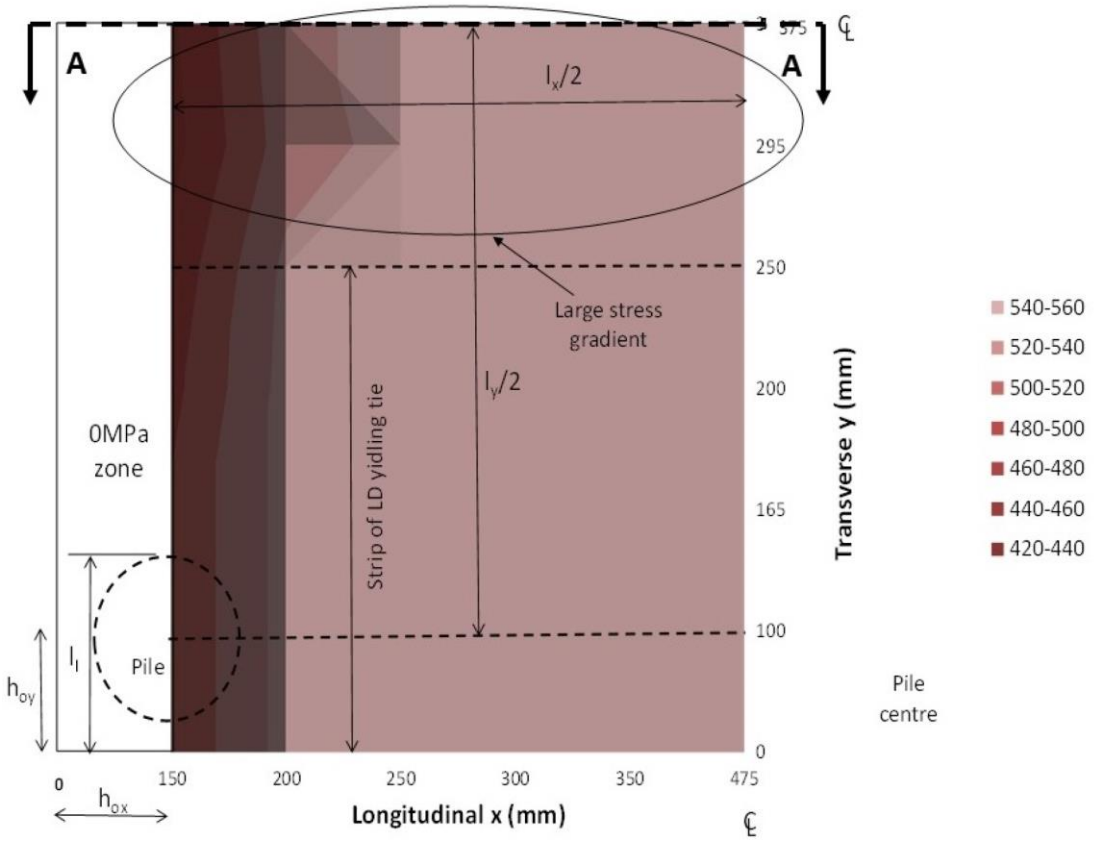


**Fig. 17** Full field LD reinforcement stress (MPa) at shear failure predicted from *S4PWv1.0* (¼ cap B4B3 $n$=5.00, $\mu$=4.23)

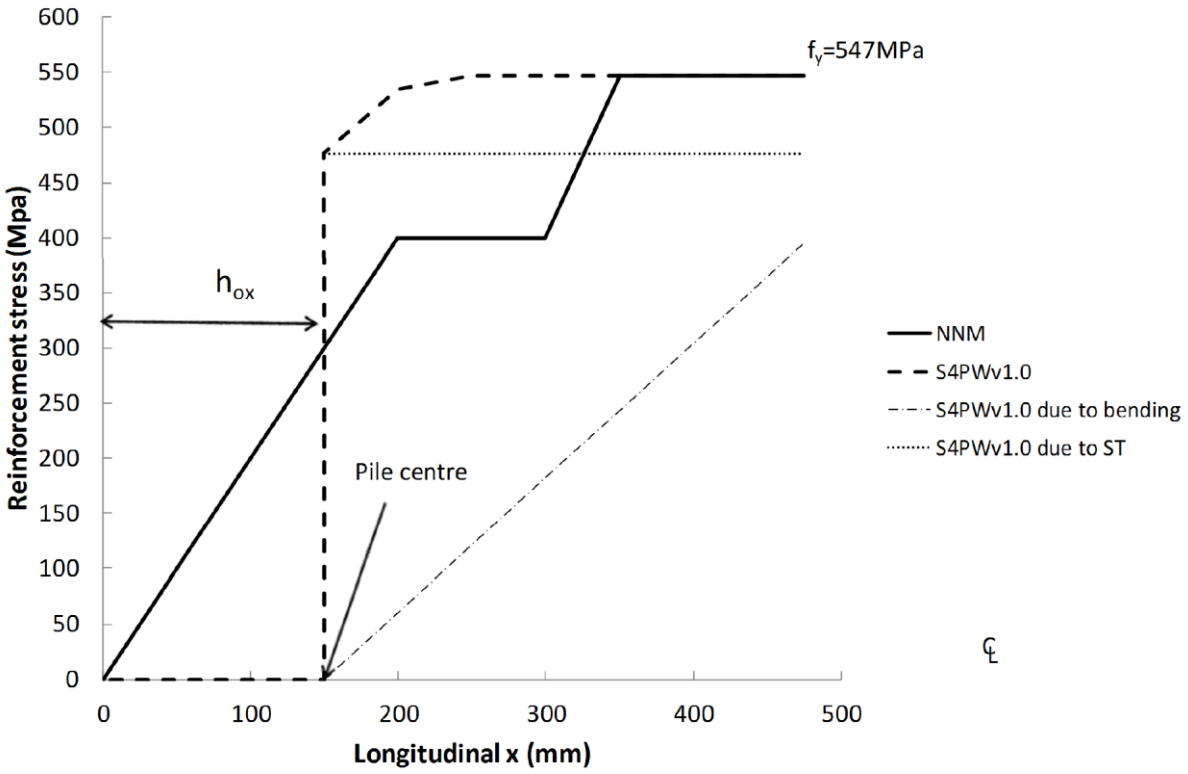


**Fig. 18** Comparison between NNM and *S4PWv1.0* for LD reinforcement stress along A-A in Figs. 3 and 17 at shear failure (cap B4B3 $n$=5.00, $\mu$=4.23)

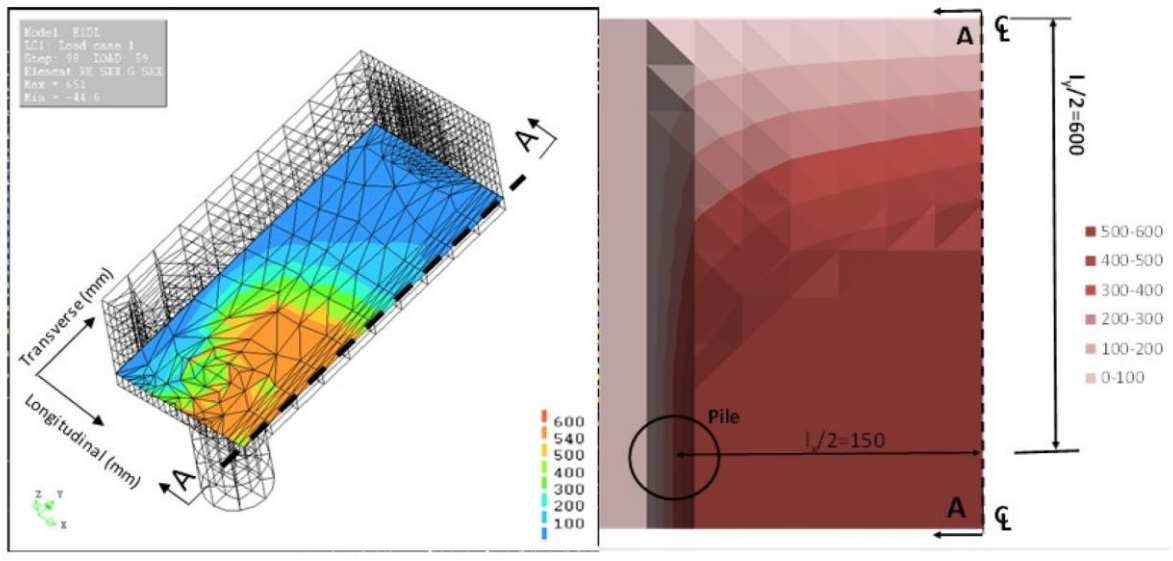


**Fig. 19** Full field LD reinforcement stress (MPa) at shear failure (¼ cap E1dl $n$=2.31 $\mu$=9.23) (left) NNM (right) *S4PWv1.0*

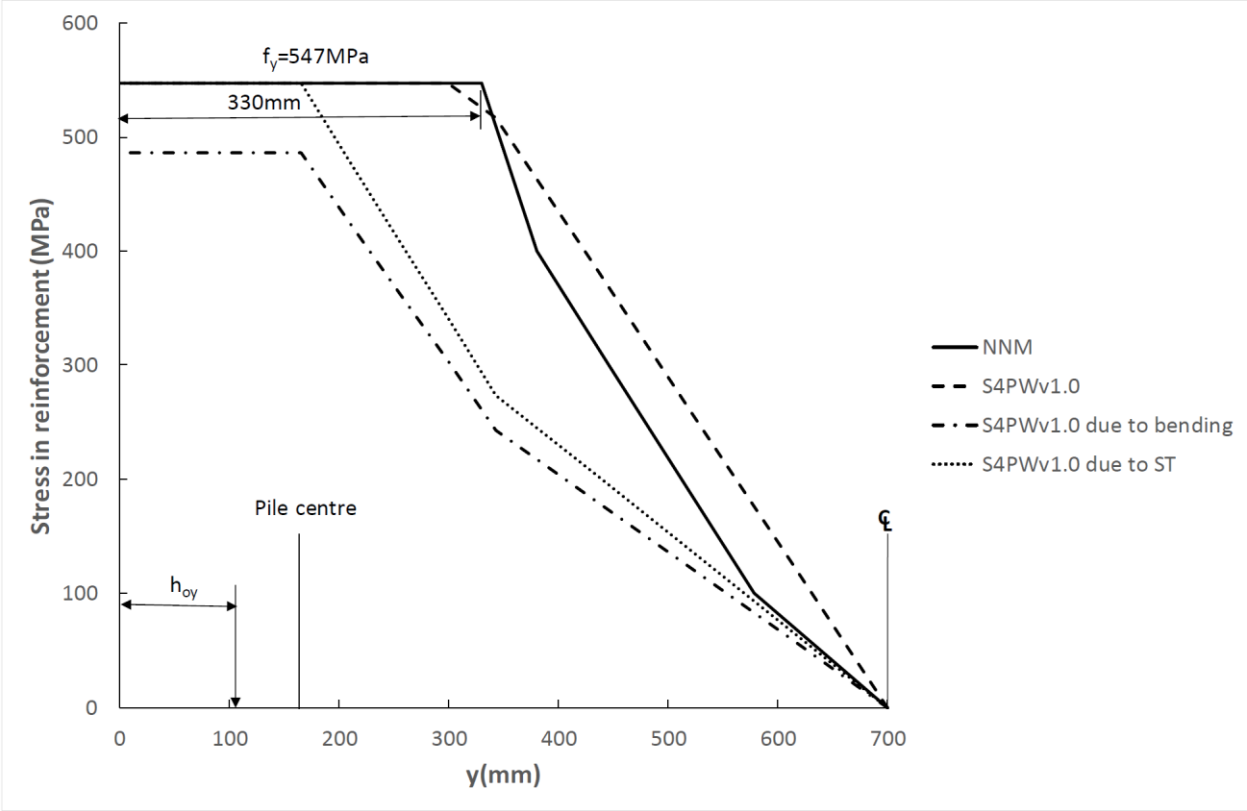


**Fig. 20** Comparison of LD reinforcement stress along A-A in Fig. 19 between NNM and *S4PWv1.0* (cap E1dl $n$=2.31 $\mu$=9.23)

Fig. 21 shows comparison of full field TD reinforcement stress distributions between NNM and *S4PWv1.0* on ¼ cap E1ej. Stress is concentrated over width $b_t=h_{ox}+l_x/4$ (Eq. 1) from both methods. Stress along A-A over the pile head is shown in Fig. 22. The stress value from *S4PWv1.0* stops at the pile inner edge, from which the shear span starts in the model, whilst the NNM gives a full width distribution. *S4PWv1.0* predicts the stress $f_y$=547MPa in the span centre. Although NNM stress reduces slightly from the pile head towards the span centre, the difference from *S4PWv1.0* is less than 47MPa.

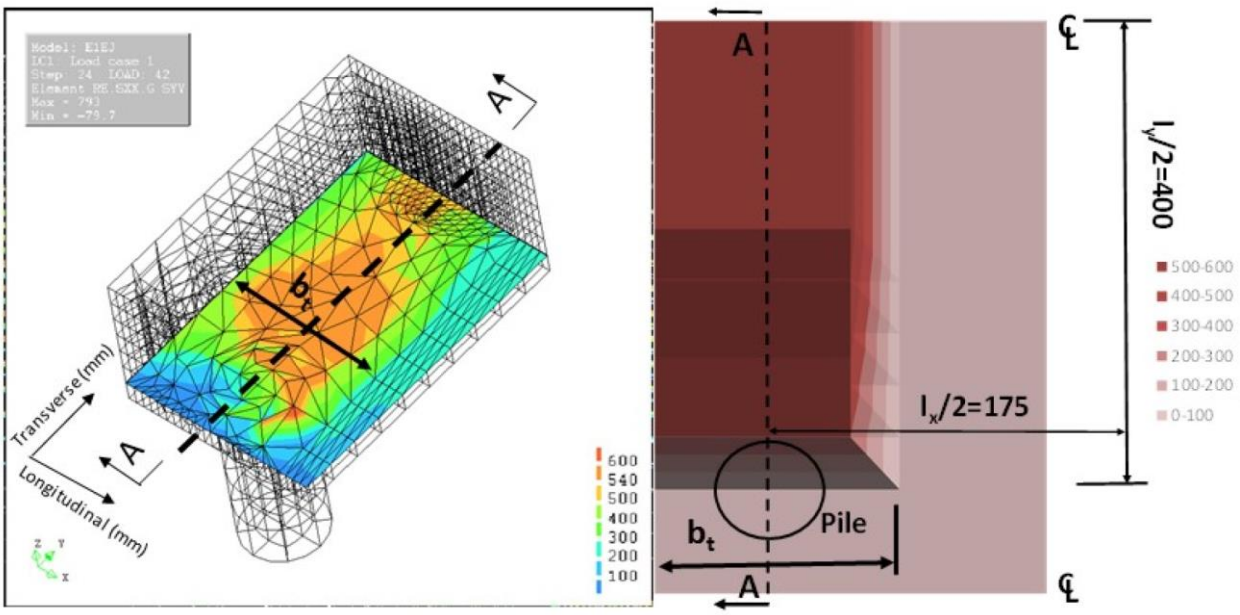


**Fig. 21** Full field TD reinforcement stress (MPa) at shear failure (¼ cap E1ej $n$=2.69 $\mu$=6.15 (left) NNM (right) *S4PWv1.0*

In Figs. 18, 20 and 22, the significant contribution of reinforcement stress from both bending and ST mechanisms is manifest. This justifies the important assumption made for the constitutive relationship of one-way RC deep beams in Eq. (13) and Eq. (16) that both mechanisms coexist in the shear behaviour.

**Evaluation of the proposed method - accuracy, efficiency and versatility**

For shear capacity for 2-way RC four-pile caps under wall loading, international standards provide three design methods, namely (i) Punching shear design method (BSI 2010; ACI 2014); (ii) Shear enhancement width method (BSI 1990, 1997, 2010) and (iii) 3-D STM assisted by elastic numerical modelling or NNM (BSI 2010; AASHTO, 2012; ACI, 2014). Method (ii) (BSI 1997) using 2-D STM, with tie width maximum three times pile diameter centred over piles, is compared with the NNM parametric study of 88 numerical cap samples and UoS experiments in Figure 23. This shows that

STM underestimates the shear capacity, especially for the circled cases with large LD pile spacing where the actual width of LD yielding tie in ST mechanism (refer Fig. 3) is larger than $3h_p$. Considering the good match between S4PWv1.0 and NNM shown in Fig. 16, the proposed method is more accurate than the existing design method.

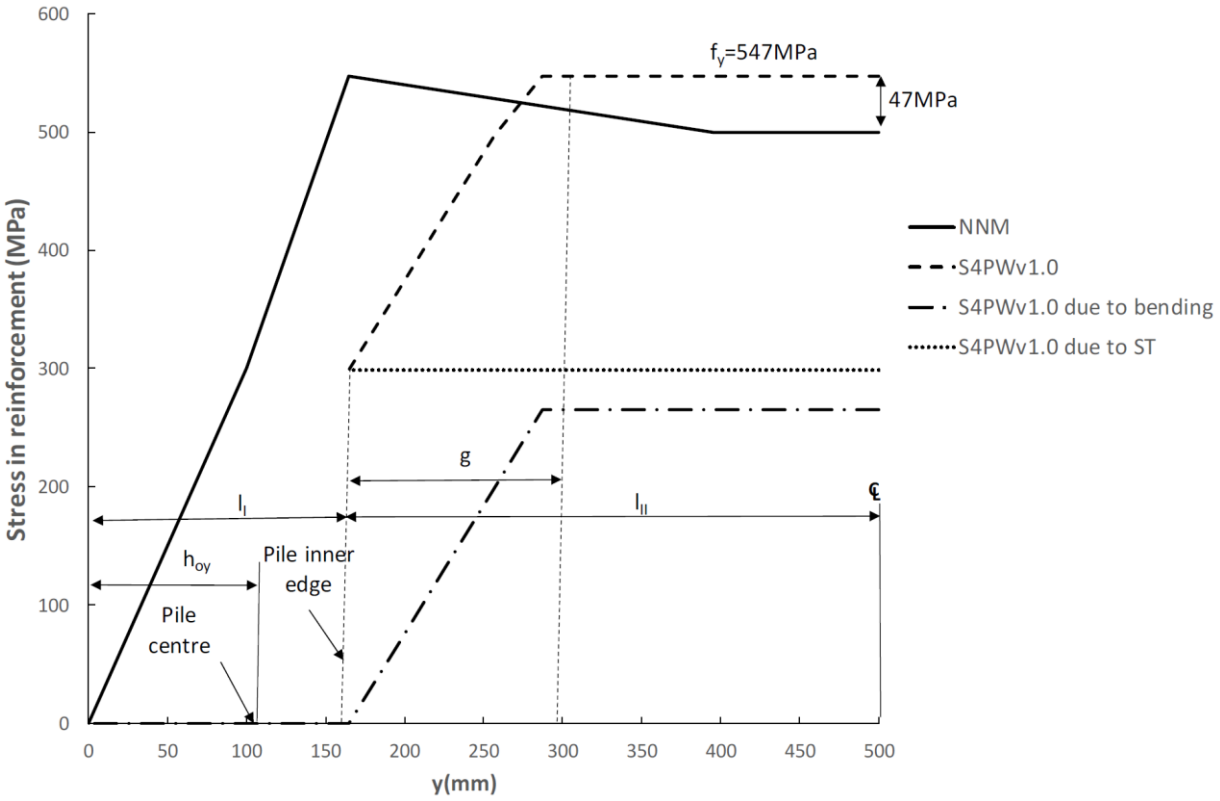


**Fig. 22** Comparison of TD reinforcement stress along A-A in Fig.21 from NNM and *S4PWv1.0* (cap E1ej $n$=2.69 $\mu$=6.15)

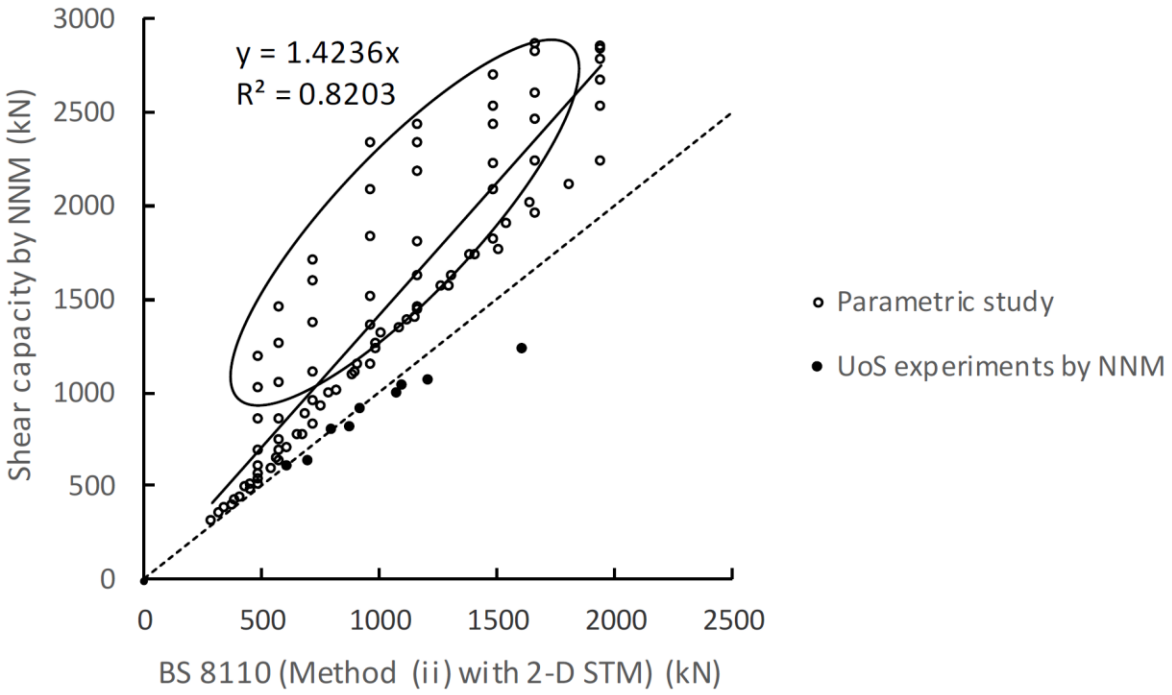


**Fig**. **23** Comparison for the parametric study and UoS experiments between NNM and BS 8110 (Method (ii) with 2-D STM)

Method (iii) utilizes lower bound plastic theory based 3-D STM. For caps under concentrated loading, the maximum load capacity solution - the pyramidal topology of the compressive struts, nodal and tension zones can be easily visualized (e.g. Mathern et al., 2017). However, for caps under wall loading, the load path topology will be fan-shaped spreading to the piles, which is difficult to visualize. Engineers may search for the optimal topology or obtain the shear capacity directly from elastic or NNM in various commercial software, where a recent development involves employing evolutionary structural optimization to identify the critical load path (Leu et al., 2006; Hardjasaputra, 2015). However, the accuracy from such models is not justifiable because of the paucity of published data to enable rigorous verification, and the limited bank of material properties and solvers for non-linear procedures in the software. Although a rigorous

NNM procedure using research-oriented software and verified carefully against test data was demonstrated in Cao (2009), it was resource intensive requiring 12 hours computational time per cap case. S4PWv1.0 achieves the balance between accuracy and time efficiency by establishing a fast design solution (in matter of seconds) of a model backed by test observation and verified by NNM. In representing the true structural shear behaviour, naturally both reinforcement stress and cap deformation can be obtained by the method, which is another advantage over existing empirical design tools.

For versatility of the proposed method and software, a straightforward extension of the application of the model and *S4PWv1.0* (Fig. 14) is to solve the shear capacity for two-row multi-pile foundations under a bridge pier wall subjected to uniform vertical traffic loading transferred through guided pot bearings (Fig. 24). Along TD, the foundation can be divided into two end caps and series of internal caps assigned with cap length $l_I$ and $l_{II}$. The total shear capacity is the summation of the shear capacity for each individual cap, which can be solved by *S4PWv1.0* directly (e.g. see $\frac{A_I}{2f(\rho_I)}$, $\frac{A_{II}}{2f(\rho_{II})}$ in Eq. (32)).

With minor adaptation, *S4PWv1.0* can also be extended to the caps with different orthogonal reinforcement ratio (i.e. $\rho_I$, $\rho_{II}$ in LD and $\rho_{III}$ in TD, which are independent in the solution, refer Figures 9 and 6) and to predict reinforcement stress and cap deformation at any loading stage $P$ prior to shear failure load $P^*$.

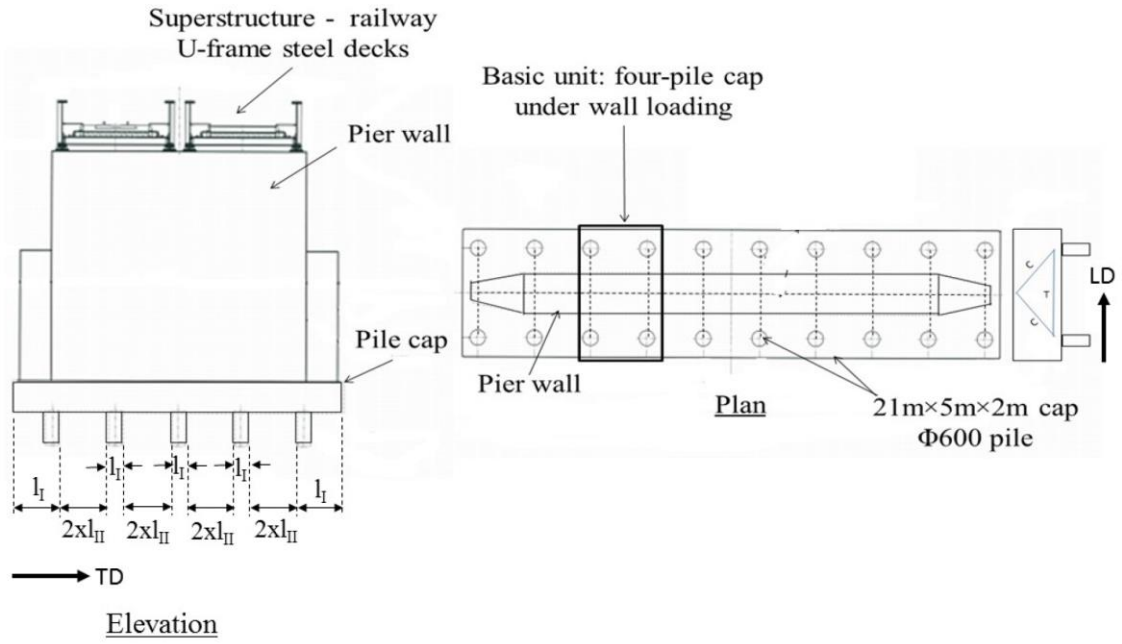


**Fig. 24** Two-row multi-pile foundation under pier wall for mining wagon train carrying bridges in Western Australia

The proposed grillage model provides researchers with a pathway for developing solutions and practical software for RC D-region structures in general under any geometry and loading configurations, provided the following criteria are satisfied, as this study has demonstrated: (i) The structure's spatial deformation under external loading can be decomposed into 1-way RC deep beams aligned with the direction of their main reinforcement; (ii). Boundary conditions including external loading displacement are quantifiable so that geometry compatibility can be established; (iii) Failure criterion for the decomposed 1-way RC deep beams related to their width is quantifiable. Either tests or advanced NNM would be needed for the proposed configuration to confirm these criteria and the final solution will be individual case based, but the pathway provides a way to solution for a wide range of structures.

An illustrative example, which meets the three criteria above, is the four-pile cap under wall loading subject to an asymmetrically applied line load *P* along TD ($l_{bx1}>l_{bx2}$) and to the distributed biaxial moments $M_x$ and $M_y$ (Figs. 25-26). In LD (Fig. 25), $\delta_b$ and $\delta_{st}$ is calculated in similar way to Eq. 13 but with the following extra consideration:

1. $\delta_b$ calculated according to the asymmetric location for *P*.
2. $\delta_{st}$ shortened by compression force $P_1'$ or $P_2'$, both of which is derived on the assumption that the cap is simply supported. Therefore, e.g. $P'_2=P(l_{bx1}+0.25h_c+0.3h_p)/l_x+M_y/l_x$.
3. The deformed angle $\alpha_1$ and $\alpha_2$ (refer $\alpha$ in Fig. 8) is obtained separately for the left and right half cap.

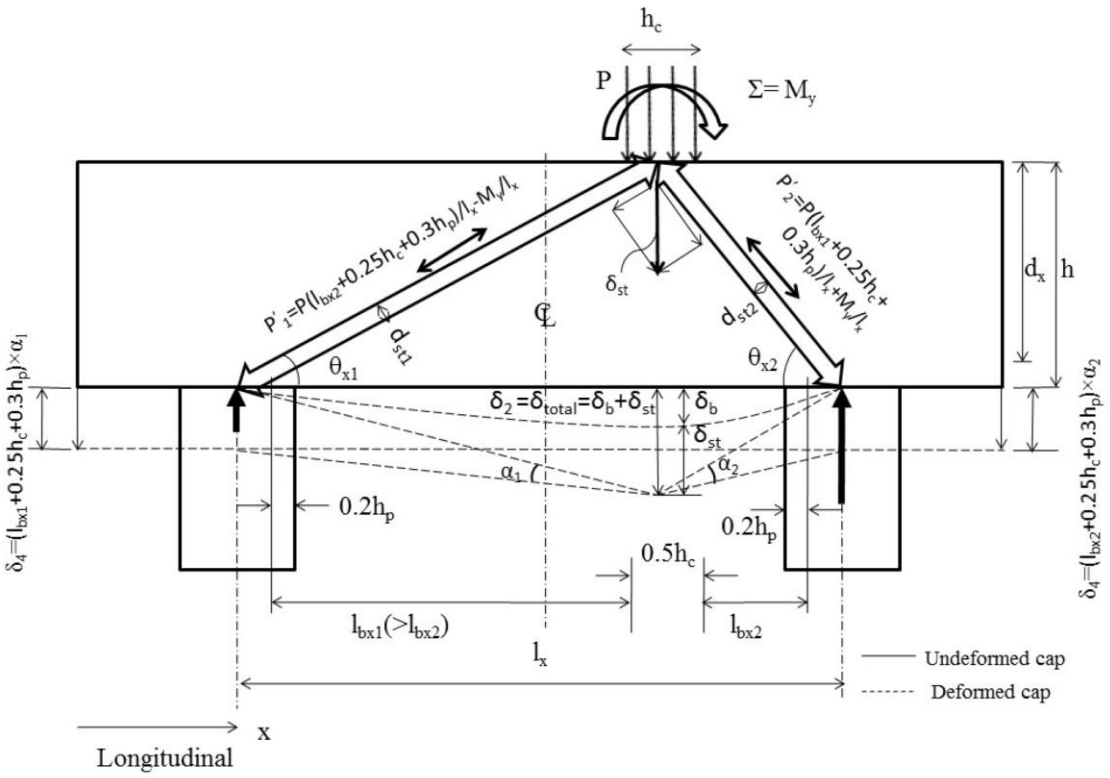


**Fig. 25.** Grillage elements and externally applied force seen from cap front surface for combined biaxial moments and wall loading

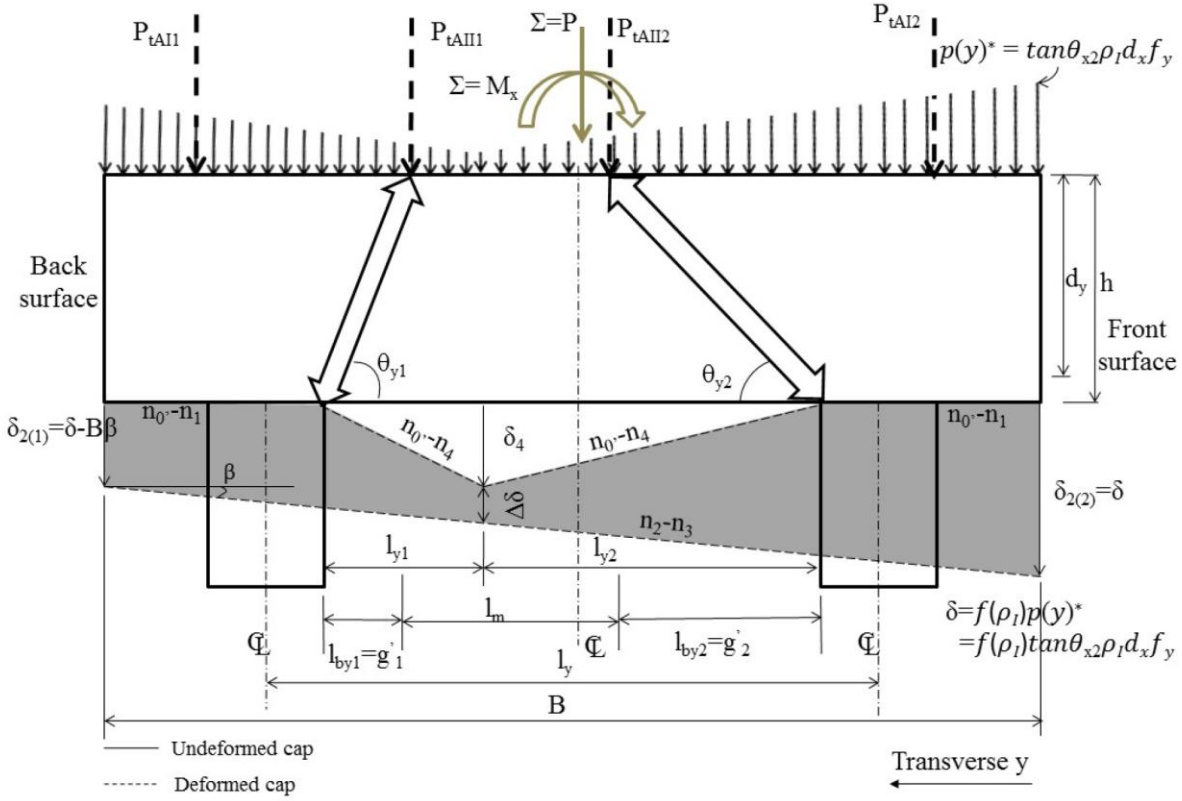


**Fig. 26.** Grillage elements and forces to TD elements seen from cap side surface for combined biaxial moments and wall loading

In TD (Fig. 26), the level deformed cap along $n_2$-$n_3$ in Figs. 9-10 is now with a slope $\beta$ due to the introduction of $M_x$. Assuming linear deformation, cap deflection $\delta_2$ in the front and back cap surface is $\delta$ and $\delta$-$B\beta$, respectively, where $B$ is the cap TD length. The failure criterion is then for reinforcement tie at cap front surface to yield at $f_y$, i.e. when $p(y)^* = tan\theta_{x2}\rho_I d_x f_y$ or $\delta = f(\rho_I)tan\theta_{x2}\rho_I d_x f_y$ is reached (refer Eqs. 28-29). To obtain the solution, the additional unknown $\beta$ can be solved by the condition that $\delta_4$ equals for both front and back half caps, bounded at intersection of $l_{y1}$ and $l_{y2}$.

For wall loading with intermediate length, the grillage model may apply allowing certain neglection of non-orthogonal cap deformation. For a cap under wall loading in length of $a$($<B/2$) in Fig. 27, where the cap deformation radiating from node $n_3'$ is not aligning with main orthogonal reinforcement, the grillage model may be implemented by introducing an additional discrete element $n_4''$-$n_3''$ with width of ($B/2$-$a$) in LD only. The element deforms under a force $Q$ at midway transferred from node $n_3'$. Solution can then be obtained in similar way, by establishing force balance, geometric compatibility and constitutive relationship together with the failure criterion observed from test and/or NNM.

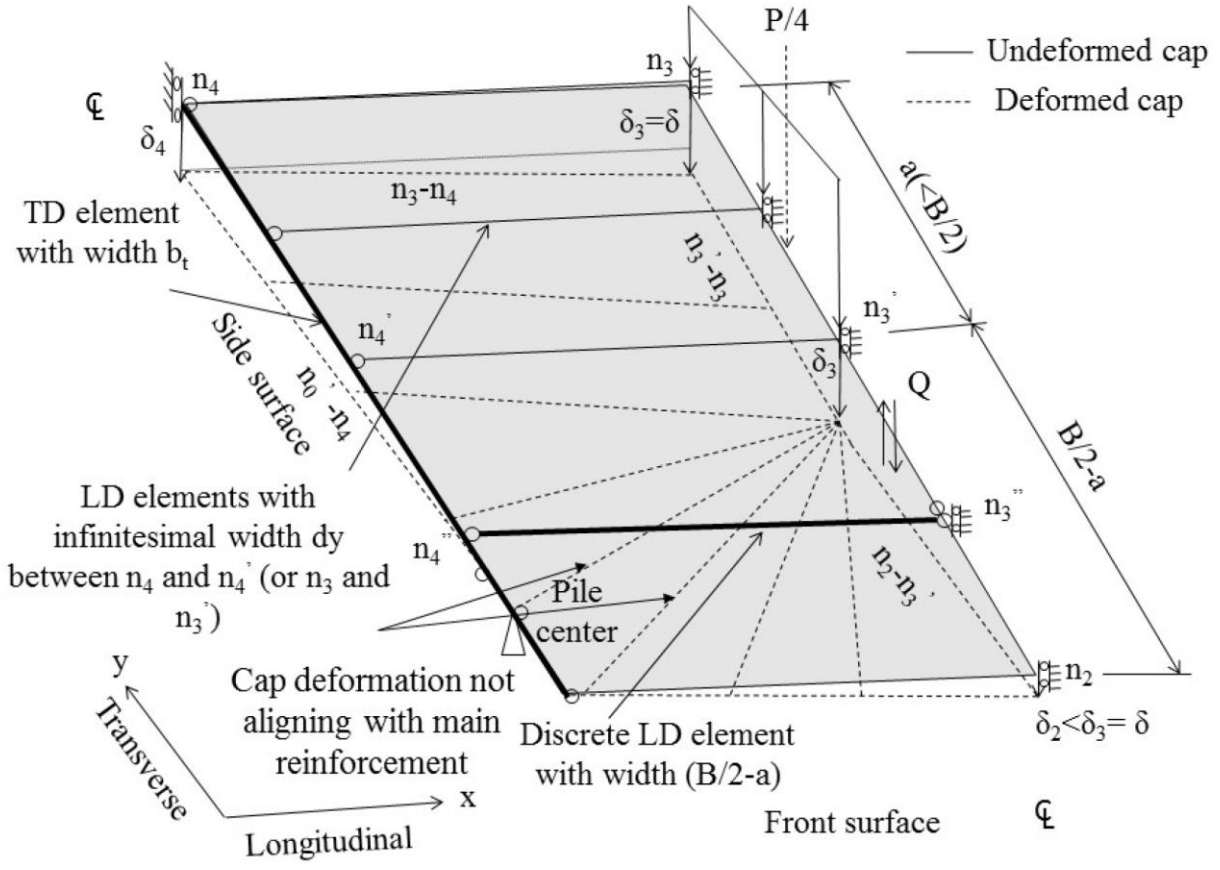


**Fig.27.** Proposed grillage model for wall loading with intermediate length

## Conclusions

Based on test observations of real shear behavior of pile caps, this paper develops an efficient tool for general daily design application, through solving a two-way statically determinate grillage model. A well verified linear load-deflection relationship for one-way RC deep beams is adopted as the constitutive relationship for the grillage elements. A VBA Userform based design software has been developed, enabling designers to obtain within seconds for each cap, the shear capacity, full field distribution of reinforcement stress and cap deflection at any design loading including the failure load. Therefore, the new method is more accurate and time efficient than the existing design tools. The proposed method has been verified for four-pile caps under wall loading but also innovates a pathway that is versatile for analyzing a wide range of two-way RC deep structural elements under various loading conditions, for which no previous international study has been performed.

## Notation

*The following symbols are used in this paper:*

$A_{II}$= area of δ(y) under length $l_{II}$;

$A_I$= area of δ(y) under length $l_I$;

$A_{st}$=reinforcement area;

$B$=cap width or deep beam width;

$b_t$=width of transverse grillage elements $n_1$-$n_0$-$n_{0'}$ and $n_{0'}$-$n_4$;

$d$= pile cap or deep beam effective depth;

$d_x$=effective pile cap depth in LD;

$d_y$=effective pile cap depth in TD;

*dy*=infinitesimal width of LD elements;

$E_c$=short term nominal concrete Young's modulus;

$E_s$=reinforcement Young's modulus;

$f_c'$=concrete compressive cylinder strength;

$f_y$=reinforcement yield strength;

*g*=distance of centroid of area $A_{II}$ from the inside face of piles;

*g'*= centroid distance of distributed wall loading *p(y)* acting on length $l_{II}$ from pile inside face;

*h*= total pile cap or deep beam depth;

$h_c$ =width of wall loading;

$h_p$= Pile diameter or width of beam support steel plate;

$h_{ox}$=cap overhang in LD;

$h_{oy}$=cap overhang in TD;

*L*=pile cap length;

$l_b$=deep beam or pile cap effective span;

$l_{bx}$ =cap effective span in LD;

$l_{by}$=cap effective span in TD;

$I_{cr}$= Second moment of area of cracked beam cross-section;

$l_l$= transverse width between outside face of cap and inside face of piles;

$l_{II}$ =transverse width between inside face of piles and cap transverse centerline (when $\delta_4 <= \delta$);

$l_m$=intermediate beam segment under uniform bending moment under 4PL;

$l_x$=pile spacing in LD or deep beam support centre spacing;

$l_y$=pile spacing in TD;

$I_{ef}$= equivalent second moment of area of pile cap or deep beam cross-section;

$n=l_x/h_p$ longitudinal pile spacing to pile diameter ratio;

$p(y)$, $p(y)^*$ =general wall loading intensity and intensity at shear failure on ¼cap, respectively;

$P$, $P^*$=total external wall load and load at shear failure on pile caps or deep beams, respectively;

$P_{lAI}$, $P_{lAII}$=resultant force acting on LD elements in ¼ cap over widths $l_I$ and $l_{II}$ respectively;

$P_{tAI}$, $P_{tAII}$=resultant force acting on TD elements in ¼ cap over widths $l_I$ and $l_{II}$ respectively;

$f(\rho_I)$, $f(\rho_{II})$=flexibility of longitudinal grillage elements per unit width under $l_I$ and $l_{II}$ respectively;

$f(\rho_{III})$=flexibility of transverse grillage elements;

$\alpha$= deformed angle of the grillage/cap soffit along TD projected onto cap front surface;

$\Delta\delta$=relative deflection between $n_4$ and $n_3$;

$\delta_4$=deflection of grillage element $n_{0'}$-$n_4$ at $n_4$;

$\delta$=constant deflection of cap under wall loading along grillage element $n_2$-$n_3$;

$\delta(y)$=midspan deflection of LD elements as a function of transverse distance $y$;

$\varepsilon_0'$=concrete compressive strain at peak compressive stress;

$\vartheta_x$=concrete strut angle in LD relative to horizontal;

$\vartheta_y$=concrete strut angle in TD relative to horizontal;

$\mu=l_y/h_p$ transverse pile spacing to pile diameter ratio;

$\rho$, $\rho_I$, $\rho_{II}$ , $\rho_{III}$ =reinforcement ratio LD elements under $l_I$ and $l_{II}$ respectively and in TD element

**Appendix 1**

The second term of Eq. (13) measures the flexibility by ST mechanism of a one-way RC deep beam under 3PL. (CIRIA 1977) assumes that ST vertical deflection $\delta_{st}$ is a component of strut shortening $\delta_s$, *i.e.* $\delta_{st,CIRIA} = \delta_s sin\vartheta_x$ (Fig.6). This paper takes a different approach that $\delta_{st}$ is a resultant of strut shortening $\delta_s$ plus a displacement due rotation of the strut around its lower end (Fig.6), i.e

$$\delta_{st} = \frac{\delta_s}{\sin\theta_x} \quad (33)$$

The shortening of the concrete struts $\delta_s = l_{st} \times \varepsilon_c$ (34)

Where $l_{st} = \frac{h}{sin\theta_x}$, the length of the concrete strut and $\varepsilon_c$ is the compressive strain in the strut.

Substitute Eq. (34) into Eq.(33), $\delta_{st} = \frac{h\varepsilon_c}{sin\theta_x{}^2}$ (35)

Now considering an internationally adopted nonlinear parabolic concrete compressive stress-strain relationship (BSI 2010; ACI 2011; Standards Australia 2009; Hognested 1951; Waner, Rangan, Hall and Faulkes 1998) , i.e.:$f_c = f_c' \left[2\left(\frac{\varepsilon_c}{\varepsilon_o'}\right) - \left(\frac{\varepsilon_c}{\varepsilon_o'}\right)^2\right]$ (36)

Where $f_c'$ (<50MPa) is the concrete cylinder strength. $\varepsilon_o'$ is the strain (=0.002) when $f_c'$ is reached.

Rearranging Eq. (36), $\varepsilon_c = (1 - \sqrt{1 - \frac{f_c}{f_c'}})\varepsilon_o'$ (37)

Substituting Eq.(37) into Eq. (35), $\delta_{st} = \frac{h(1-\sqrt{1-\frac{f_c}{f_c'}})\varepsilon_o'}{sin\theta_x{}^2}$ (38)

From ST force equilibrium against yielding reinforcement, the force in the compressive strut when strut-and-tie fails, $P' = \frac{A_{st}f_y}{\cos\theta_x}$ (39)

Where $A_{st}$ and $f_y$ is the area and yielding strength of LD reinforcement, respectively.

Now assume the concrete strut is in a prism with constant width of $d_{st}$ (Fig. 6) which stays invariant in any loading stage. Denoting strut width as $B$, $d_{st}$ is derived from Eq. (39),

$$d_{st} = \frac{P'}{f_c' \times B} = \frac{A_{st} f_y}{f_c' \times B \times \cos\theta_x} \quad (40)$$

On the other hand, load allocated to each concrete strut in any loading stage P (Fig.6) is $\frac{P}{2\sin\theta_x}$.

The corresponding compressive stress in concrete strut $f_c = \frac{P}{2\sin\theta_x \times d_{st} \times B}$ (41)

Substitute Eq.(40) into Eq.(41), $f_c = \frac{P}{2\sin\theta_x \times \frac{A_{st} f_y}{f_c' \times B \times \cos\theta_x} \times B} = \frac{P f_c'}{2\tan\theta_x \times A_{st} f_y}$ (42)

Substitute Eq. (42) into Eq. (38), $\delta_{st} = \frac{\varepsilon_o' h (2 - \sqrt{4 - \frac{2P}{A_{st} f_y \tan\theta_x}})}{2\sin\theta_x^2}$ (43)

Eq.(43) gives a constitutive $P$-$\delta_{st}$ load-deflection relationship, considering an ideal compressive stress-strain curve given by Eq.(36). However, to solve the grillage model more efficiently, this study showed practically that a linear $P$-$\delta_{st}$ relationship was deemed to be warranted.

Now downgrade parabolic Eq.(37) to a linear format, i.e. compressive strain $\varepsilon_c$ in the concrete strut in any loading stage is directly proportional to compressive stress $f_c$, $\varepsilon_c = \frac{\varepsilon_o'}{f_c'} f_c$ (44)

Substituting Eq.(44) into Eq.(35), $\delta_{st} = \frac{h\frac{\varepsilon_o'}{f_c'} f_c}{\sin\theta_x^2}$ (45)

Further replace $f_c$ in Eq.(45) with Eq.(42), $\delta_{st} = \frac{\varepsilon_o' h}{2\sin\theta_x^2 \tan\theta_x \times A_{st} f_y} P$ (46)

Eq.(46) becomes the second term of Eq. (13).

**References**

AASHTO (American Association of State Highway and Transportation Officials) (2012). "AASHTO LRFD Bridge Design Specifications. " *AASHTO, Washington, DC,* U.S.A.

ACI (American Concrete Institute) (2011). “Building Code Requirements for Structural Concrete and Commentary, ACI 318-11.” *ACI:* Farmington Hills, U.S.A.

ACI (American Concrete Institute) (2014). "ACI 318-14 Building Code Requirements for Structural Concrete." *ACI*: Farmington Hills, Michigan, U.S.A.

Bloodworth, A.G., Cao, J. and Xu, M. (2012). “Numerical modeling of shear behavior of reinforced concrete pile caps.” *J. Structural Eng.*, 10.1061/(ASCE)ST.1943-541X.0000499.

BSI (British Standards Institution) (1990). "BS 5400-4 Steel, Concrete and Composite Bridges-Part 4: Code of Practice for Design of Concrete Bridges." *BSI:* Milton Keynes, UK.

BSI (British Standards Institution) (1997). "BS 8110-1 Structural Use of Concrete-Part 1: Code of Practice for Design and Construction." *BSI:* Milton Keynes, UK.

BSI (British Standards Institution) (2004). “BS EN 1992-1-1: 2004 - Design of concrete structures – Part 1-1: General rules and rules for buildings.” *BSI:* London, UK.

BSI (British Standards Institution) (2005). “BS EN 1992-2: 2005 - Design of concrete structures – Part 2: Concrete bridges – Design and detailing rules.” *BSI:* London, UK.

BSI (British Standards Institution) (2010). “BS EN 1992-1-1:2004 - Eurocode 2: Design of concrete structures - Part 1-1: General rules and rules for buildings.” *BSI:* London, UK.

Cao, J. (2009). “The shear behavior of the reinforced concrete four-pile caps.” *PhD thesis*, *University of Southampton*, *UK*.

Cao, J., and Bloodworth, A. G. (2012). “Shear behaviour of reinforced concrete pile caps under full-width wall loading.” *Proc. ICE Structures and Buildings*, 165(4), 165–177.

CIRIA (Construction Industry Research and Information Association) (1977). CIRIA Guide 2 - The design of deep beams in reinforced concrete beams. London, UK.

Clarke, J. L. (1973). “Behaviour and Design of Pile Caps with Four Piles, Technical Report.” *Wexham Springs: Cement and Concrete Association*, 124-136.

De Paiva, H.A.R. and Austin, W.J. (1960). “Behaviour and design of deep structural members Part 3: Test of Reinforced concrete deep beams.” University of Illinois, Urbana, IL.

Hardjasaputra, H. (2015) “Evolutionary structural optimization as tool in finding strut-and-tie models for designing reinforced concrete deep beam. *The 5th International Conference of Euro Asia Civil Engineering Forum (EACEF-5)*, Procedia Engineering 125 (2015) 995-1000.

Hognestad, E. (1951). “A study of combined bending and axial load in reinforced concrete members.” *University of Illinois*, Eng. Expt. Station Bulletin, No. 399.

Kani, G. (1964). “The riddle of shear failure and its solution.” *ACI Journal,* 61(4), 441-467.

Kotsovos, M.D. (1987). “Shear failure of reinforced concrete beams.” *Engineering Structures,* 9(1), 32-38.

Leu, L.J., Huang, C. W., Chen, C.S., Liao, Y.P. (2006). “Strut-and-tie design methodology for three-dimensional reinforced concrete structures.” *J. of Structural Eng.,* ASCE, June, 929-938.

Mathern, A., Chantelot, G., Per Kettil, P.S., Bjorn Engstrom, R.R. (2017). “Enhanced strut-and-tie model for reinforced concrete pile caps.” *39th IABSE Symposium – Engineering the future*, September 21-23 2017, Vancouver, Canada.

Mihaylov, B.I. (2015). “Five-spring model for complete shear behaviour of deep beams” *Structural Concrete*, 16(1), 71-83.

Mihaylov, B.I., Bentz, E.C., Collins, M.P. (2013). “Two-Parameter Kinematic Theory for Shear Behavior of Deep Beams” *ACI Structural Journal,* 110(3), May-June 2013.

Mihaylov, B.I., Hunt, B, Bentz, E.C., Collins, M.P. (2015). “Three-Parameter Kinematic Theory for Shear Behavior of Continuous Deep Beams” *ACI Structural Journal,* 112(1), Jan.-Feb. 2015.

Rao, G.A., Kunal, K. and Eligehausen, R. (2007). “Shear Strength of Reinforced Concrete Deep Beams.” *Proc. 6th Int. Conf. Fracture Mechanics of Concrete and Concrete Structures (FraMCoS-6)*, 693-699. Taylor and Francis.

Standards Australia. (2004). “AS 5100.5: 2004 - Bridge Design Part 5: Concrete.” *Sydney: Standards Australia.*

Standards Australia. (2009). “AS 3600: 2009 Concrete structures.” *Sydney: Standards Australia*.

Waner, R.F., Rangan, B.V., Hall, A.S. and Faulkes, K.A. (1998). “Concrete Structures.” *Longman*.

Yang, C.-J. and Jun D.-H. (2003). “A study on the shear behaviour of deep beams under point loads.” *Proc. 9$^{th}$ East Asia-Pacific Conf. on Structural Engineering and Construction*.